A role for endothelial alpha-mannosidase MAN1C1 in radiation-induced immune cell recruitment

Ségolène Ladaigue, Anne-Charlotte Lefranc, Khadidiatou Balde, Monica Quitoco, Emilie Bacquer, Didier Busso, Guillaume Piton, Jordane Dépagne, Nathalie Déchamps, Nao Yamakawa, et al.

iScience

CellPress
OPEN ACCESS

Article

A role for endothelial alpha-mannosidase MAN1C1 in radiation-induced immune cell recruitment

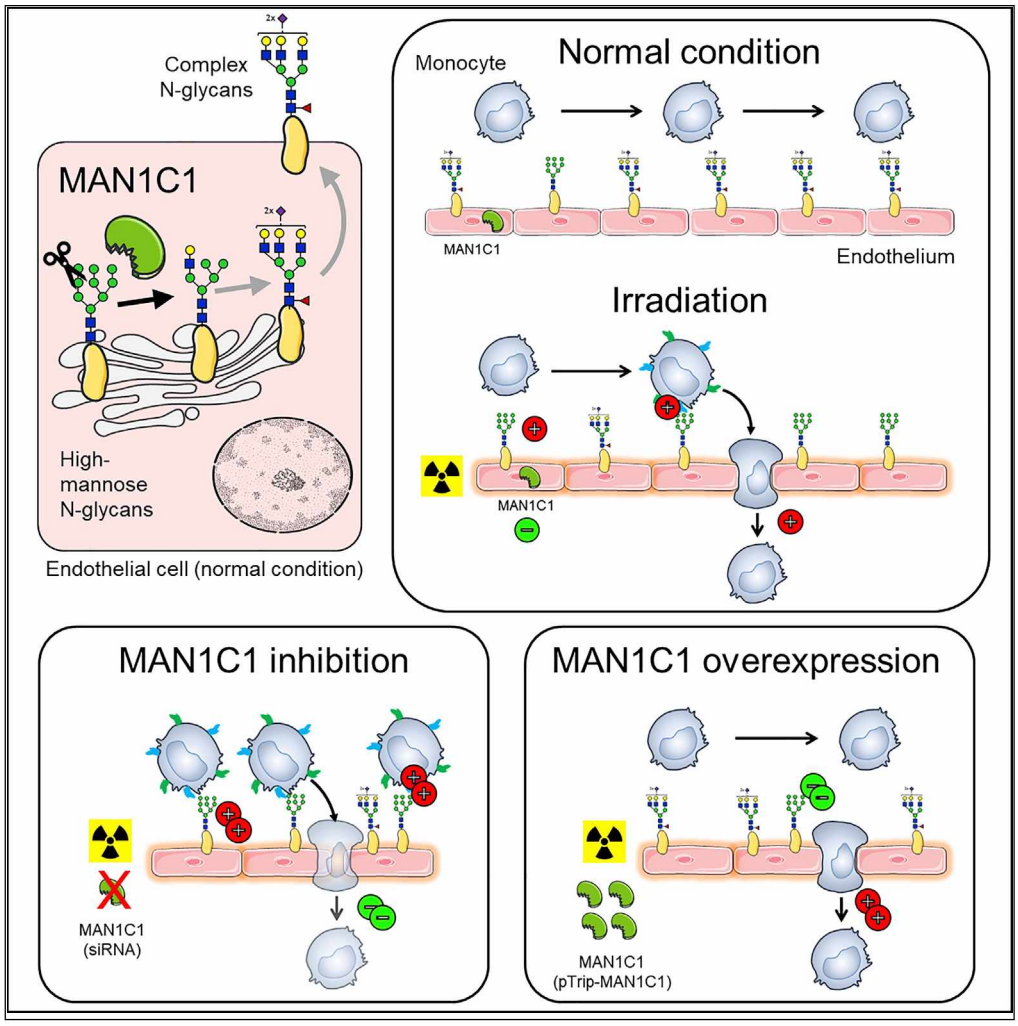

Ségolène Ladaigue, Anne-Charlotte Lefranc, Khadidiatou Balde, ..., Vincent Paget, Fabien Milliat, Olivier Guipaud

olivier.guipaud@irsn.fr

Highlights

Irradiation of endothelial cells (ECs) boosts monocyte adhesion and transmigration

Irradiation of ECs decreases the expression of class I alpha-mannosidase 1 (MAN1C1)

MAN1C1 regulates high-mannose N-glycan abundance in ECs

MAN1C1 contributes to radiation-induced interactions between ECs and monocytes

Ladaigue et al., iScience 25, 105482
December 22, 2022
https://doi.org/10.1016/j.isci.2022.105482

iScience

CellPress
OPEN ACCESS

Article

A role for endothelial alpha-mannosidase MAN1C1 in radiation-induced immune cell recruitment

Ségolène Ladaigue,[1,2] Anne-Charlotte Lefranc,[1] Khadidiatou Balde,[1] Monica Quitoco,[1] Emilie Bacquer,[1] Didier Busso,[3] Guillaume Piton,[3] Jordane Dépagne,[3] Nathalie Déchamps,[4] Nao Yamakawa,[5] Louise Debusschere,[5] Chunxue Han,[5] Fabrice Allain,[6] Valérie Buard,[1] Georges Tarlet,[1] Agnès François,[1] Vincent Paget,[1] Fabien Milliat,[1] and Olivier Guipaud[1,7,*]

SUMMARY

Radiation therapy damages tumors and normal tissues, probably in part through the recruitment of immune cells. Endothelial high-mannose N-glycans are, in particular, involved in monocyte-endothelium interactions. Trimmed by the class I α-mannosidases, these structures are quite rare in normal conditions. Here, we show that the expression of the endothelial α-mannosidase MAN1C1 protein decreases after irradiation. We modeled two crucial steps in monocyte recruitment by developing *in vitro* real-time imaging models. Inhibition of MAN1C1 expression by siRNA gene silencing increases the abundance of high-mannose N-glycans, improves the adhesion of monocytes on endothelial cells in flow conditions and, in contrast, decreases radiation-induced transendothelial migration of monocytes. Consistently, overexpression of MAN1C1 in endothelial cells using lentiviral vectors decreases the abundance of high-mannose N-glycans and monocyte adhesion and enhances transendothelial migration of monocytes. Hence, we propose a role for endothelial MAN1C1 in the recruitment of monocytes, particularly in the adhesion step to the endothelium.

INTRODUCTION

Ionizing radiation delivered during radiation therapy damages tumors and surrounding normal tissue, which may result in late effects that can reduce patients' quality of life. Such injury is partly due to the massive recruitment of immune cells, in particular macrophages, but has distinct mechanisms in normal tissue and tumors.[1–5] In this process, the irradiated vascular endothelium plays a prominent role as it is the gateway for circulating immune cells to enter injured tissues.[6,7]

Immune cell recruitment involves cell-cell specific interactions mediated by the glycosylation of surface adhesion proteins.[8] Endothelial N-glycans appear to be significantly involved in monocyte-endothelium interactions for the recruitment of monocytes during inflammation.[9] High-mannose N-glycans are immature structures generally trimmed by mannosidases under normal conditions.[10] However, in an inflammatory context triggered by TNFα stimulation, atherosclerosis or oxidative stress, these structures are more abundant and are responsible for the adhesion of monocytes to the endothelium,[11,12] at least partly through the glycosylation of intercellular adhesion molecule-1 (ICAM-1).[13,14] The glycome of endothelial cells is also profoundly altered under radiation exposure.[15] Endothelial cells exhibit a greater abundance of high-mannose N-glycans that are responsible for the radiation-induced increase in monocyte adhesion. Associated with these changes, a transcriptomic study showed a decrease in the expression of the endothelial MAN1C1 gene that encodes the class I α-mannosidase MAN1C1 protein.[15] However, the role of this enzyme in monocyte adhesion in response to a proinflammatory signal remains elusive.

In this work, we show that endothelial MAN1C1 protein expression decreases after irradiation. We observed that the inhibition of MAN1C1 expression increases the abundance of high-mannose N-glycans and promotes the adhesion rate of monocytes on endothelial cells in flow conditions. In contrast, inhibition of MAN1C1 expression impairs radiation-induced transendothelial migration of monocytes. On the other hand, MAN1C1 overexpression in endothelial cells consistently decreases the abundance of high-mannose N-glycans and monocyte adhesion on endothelial cells under flow conditions and enhances

[1]Institut de Radioprotection et de Sûreté Nucléaire (IRSN), PSE-SANTE/SERAMED/LRMed, 92260 Fontenay-aux-Roses, France

[2]Sorbonne University, Doctoral College, 75005 Paris, France

[3]CIGEx, Université de Paris, Université Paris-Saclay, Inserm, CEA, Institut de Biologie François Jacob, iRCM, UMR Genetic Stability, Stem Cells and Radiation (SGCSR), Fontenay-aux-Roses, France

[4]Institut de Biologie François Jacob (IBFJ), Institute of Cellular and Molecular Radiobiology, CEA, UMR967 INSERM, 96265 Fontenay-aux-Roses, France

[5]Université de Lille, CNRS, Inserm, CHU Lille, Institut Pasteur de Lille, US 41 - UAR 2014 - PLBS, 59000 Lille, France

[6]Université de Lille, UMR 8576 - UGSF - Unité de Glycobiologie Structurale et Fonctionnelle, 59000 Lille, France

[7]Lead contact

*Correspondence: olivier.guipaud@irsn.fr

https://doi.org/10.1016/j.isci.2022.105482

transendothelial migration of monocytes. Together, our results show a role for endothelial MAN1C1 in the adhesion of monocytes to vascular endothelium, the first essential step in immune cell recruitment.

RESULTS

The abundance of endogenous endothelial MAN1C1 protein decreases in HUVECs after irradiation

Since expression of the MAN1C1 gene decreased in human umbilical vein endothelial cells (HUVECs) following radiation exposure,[15] we wondered if protein abundance is also regulated by irradiation. HUVECs were irradiated at 20 Gy and proteins were collected at different times post-irradiation. The abundance of MAN1C1 protein was assessed by Western blot, showing a decrease in the abundance of MAN1C1 in response to ionizing radiation 2 and 4 days post-irradiation (Figures 1 and S1). To ensure the specificity of the band detected by the anti-MAN1C1 antibody, we constructed a lentiviral vector (pTrip-MAN1C1) to overproduce the Myc-tagged MAN1C1 fusion protein under the MND promoter, as well as a lentiviral vector expressing the luciferase protein (pTrip-LUC), instead of MAN1C1, as a control (Figure S2). The transduction rate was assessed by microscopy fluorescence and flow cytometry using the fluorescence of the eGFP protein expressed under the hPGK promoter (Figures S2B and S2C). Protein extracts of the transduced cells with pTrip-MAN1C1 show a strong overexpression of MAN1C1 compared to cells transduced with the control lentiviral particles (Figures 1A and S2D). Western blot analysis of proteins at later times shows that MAN1C1 expression drops even more drastically with time in irradiated HUVECs compared to unirradiated HUVECs (Figure S1B). To find out how MAN1C1 could be regulated by ionizing radiation, we used Pathway Studio software to establish relationships between the four class I α-mannosidases, MAN1A1, MAN1A2, MAN1B1 and MAN1C1, their upstream regulatory entities, and the term "Radiation" as a treatment. Figure 1C displays the putative regulatory network of the four class I α-mannosidases. The network proposes a pathway for the inhibition of MAN1C1 expression by ionizing radiation via the classical DNA repair signaling pathway that involves ATM, NF-κB, IL1B, TNFα and/or TGFβ, and through less commonly described effectors, such as miR425 and miR206 miRNAs.

Endothelial MAN1C1 is involved in radiation-induced monocyte adhesion on a HUVEC monolayer under flow conditions

Previous research showed that adhesion of THP-1 monocytes to TNFα-stimulated or irradiated HUVECs is improved under flow conditions.[11,15] This adhesion was at least partly due to the overexpression of high-mannose N-glycans at the surface of endothelial cells. MAN1C1 oversees high-mannose N-glycan trimming in the cell. To investigate the role of MAN1C1 in immune cell recruitment, we opted for a silencing and overexpression strategy to evaluate the consequences on monocyte adhesion and transendothelial migration.

We first inhibited endothelial MAN1C1 gene expression using siRNA to quantify THP-1 cell adhesion under flow conditions on a HUVEC layer irradiated at 20 Gy. At the time of the adhesion assay, *i.e.* 2 days after irradiation, the number of cells in the irradiated condition was reduced by half compared to non-irradiated cells (Figure S3), which was expected from our previous results using the same protocol.[15] However, the viability of the cells that remained adherent, at that time, was not altered, showing that the cells considered in the study are still living cells (Figure S3). At day 2 post-irradiation, the inhibition of MAN1C1 gene expression was about 90% in irradiated and non-irradiated HUVECs (Figure 2A). However, this inhibition is not detected using Western blot analysis (Figure 2B). The endogenous MAN1C1 protein is minimally expressed in HUVECs, which makes it impossible to quantify the signal decrease. Nonetheless, MAN1C1 silencing leads to an increase in high-mannose N-glycans, as shown by the quantification of the concanavalin A lectin conjugated to fluorescein isothiocyanate (FITC-Con A) by flow cytometry (Figure 2C) and quantification by liquid chromatography coupled to tandem mass spectrometry (LC-MS/MS) (Figure 2D). LC-MS/MS allowed the identification and quantification of the relative abundances of 5 different high-mannose N-glycans and 4 different complex N-glycans (Figure S4). It highlights an increase of the high-mannose structures, particularly for irradiation conditions, at the expense of the complex structures, which was logically expected considering the biosynthesis pathway of N-glycans. We then evaluated the effect of MAN1C1 inhibition on monocyte adhesion under flow conditions. The results show a significant increase in adhesion compared to HUVECs transfected with a control siRNA under non-irradiated conditions (Figures 2E, 2F, and Video S1). The levels of adhesion are equivalent in unirradiated and irradiated samples, suggesting that the increase due to MAN1C1 inhibition cannot be greater.

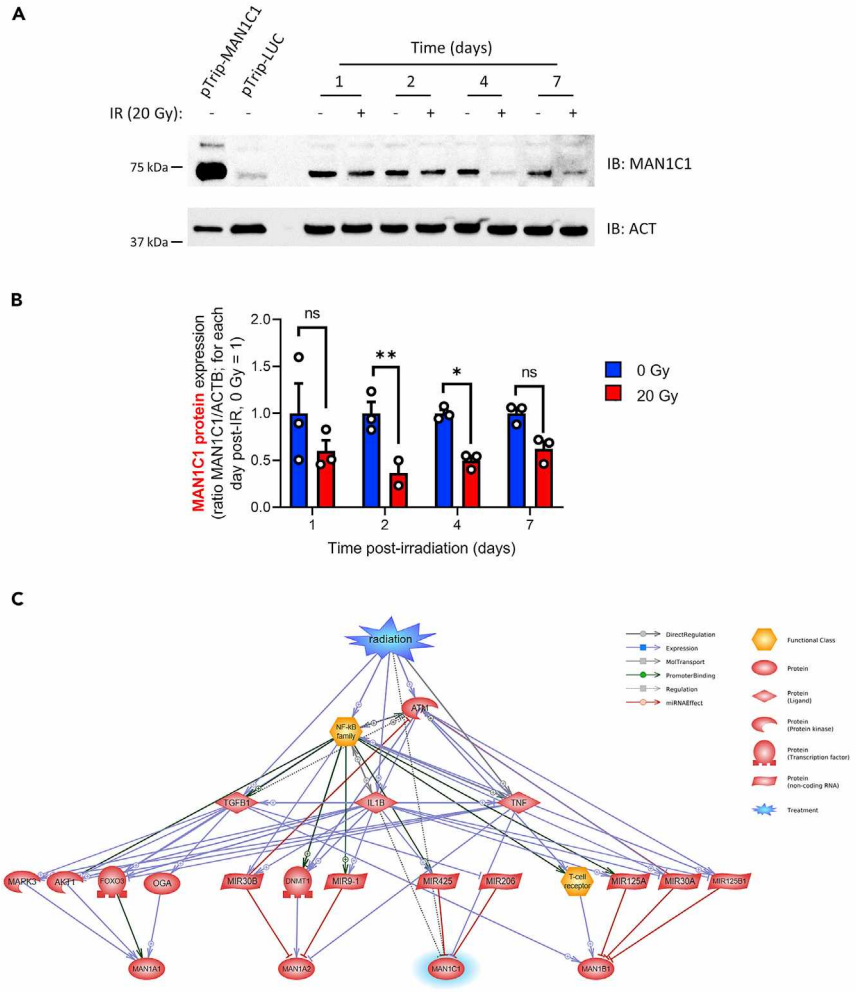

Figure 1. The endogenous MAN1C1 protein is downregulated in HUVECs after irradiation

HUVECs were irradiated at 20 Gy or not irradiated, and proteins were collected 1, 2, 4, and 7 days after irradiation. To produce a positive control of the MAN1C1 signal on the Western blot membrane, HUVECs were transduced with the pTrip-MAN1C1 or the pTrip-LUC lentiviral particles.

(A) Representative Western blot images performed with anti-MAN1C1 and anti-Actin B antibodies on HUVEC protein extracts (15 μg). pTrip-LUC and p-Trip-MAN1C1, protein extracted (2 μg) of transduced cells with the corresponding lentiviral vectors. IB, immunoblot.

(B) Relative densitometric bar graphs of ratio MAN1C1/ACTB. Data are represented as mean ± SEM of three independent samples for each day post-irradiation. One-way ANOVA test with Sidak correction. ns, not significant, *$p \leq 0.05$, **$p \leq 0.01$.

(C) Overview of the putative regulatory network of class I α-mannosidases. Relationships between the four class I α-mannosidases, MAN1A1, MAN1A2, MAN1B1, and MAN1C1, their upstream regulatory entities, and the term "Radiation" as a treatment are shown by directional arrows (see legend on the right panel). Direct interactions and shortest paths were used to construct the network established using the literature mining algorithm of Pathway Studio software. MAN1C1 is highlighted in blue.

See also Figures S1 and S2.

We then used the reverse strategy, by overexpressing the MAN1C1 protein with the lentiviral vector we constructed (Figure 3). The results show a significant MAN1C1 overexpression at the time of THP-1 monocyte adhesion assay under flow conditions (Figure 3A). Associated with MAN1C1 overexpression, analysis of the N-glycan content of endothelial proteins by LC-MS/MS shows a statistically significant decrease in high-mannose N-glycans, associated with an increase in complex N-glycans, both in non-irradiated and irradiated conditions (Figure 3B). Importantly, this decrease in high-mannose N-glycan abundance

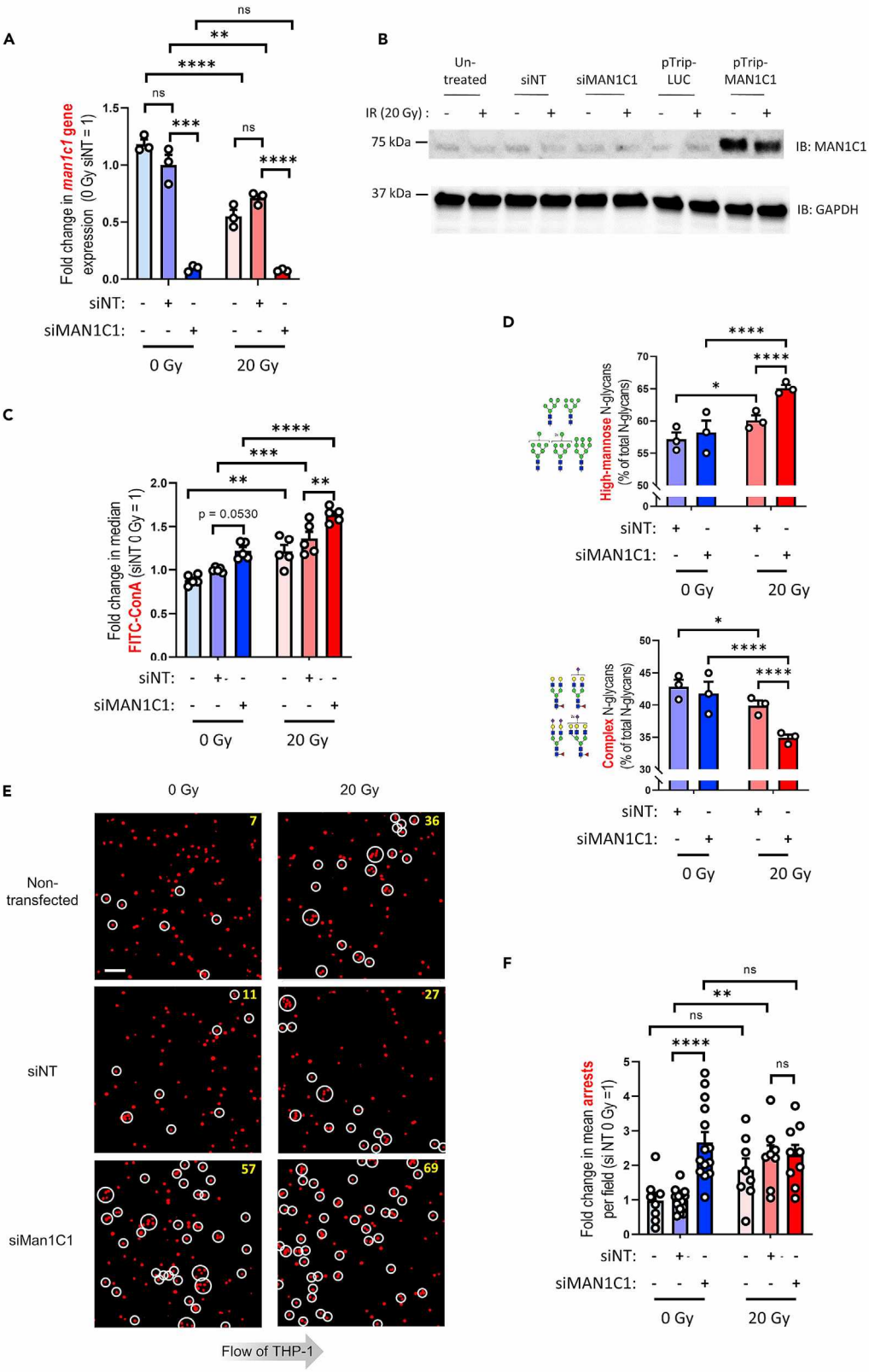
A
ns
**
****
ns
***
ns
****
Fold change in man1c1 gene expression (0 Gy siNT = 1)
1.5
1.0
0.5
0.0
siNT: - + - - + -
siMAN1C1: - - + - - +
0 Gy
20 Gy
B
Un-treated
siNT
siMAN1C1
pTrip-LUC
pTrip-MAN1C1
IR (20 Gy) : - + - + - + - + - +
75 kDa
IB: MAN1C1
37 kDa
IB: GAPDH
C
****
***
**
**
p = 0.0530
Fold change in median FITC-ConA (siNT 0 Gy = 1)
2.0
1.5
1.0
0.5
0.0
siNT: - + - - + -
siMAN1C1: - - + - - +
0 Gy
20 Gy
D
****
****
*
High-mannose N-glycans (% of total N-glycans)
70
65
60
55
50
0
siNT: + - + -
siMAN1C1: - + - +
0 Gy
20 Gy
*
****
****
Complex N-glycans (% of total N-glycans)
50
45
40
35
30
0
siNT: + - + -
siMAN1C1: - + - +
0 Gy
20 Gy
E
0 Gy
20 Gy
Non-transfected
siNT
siMan1C1
7
36
11
27
57
69
Flow of THP-1
F
ns
**
ns
****
ns
Fold change in mean arrests per field (si NT 0 Gy = 1)
5
4
3
2
1
0
siNT: - + - - + -
siMAN1C1: - - + - - +
0 Gy
20 Gy

Figure 2. Increased monocyte adhesion under flow conditions on a HUVEC monolayer treated with siRNA against MAN1C1

HUVECs were transfected with siRNA against MAN1C1 (siMAN1C1) or non-targeted siRNA (siNT). Three days post-transfection, cells were irradiated at 20 Gy, or not irradiated. Two days post-irradiation, proteins, and RNAs were collected for Western blot and RT-qPCR analysis, cells were labeled with FITC-Con A to assess the level of high-mannose N-glycans by flow cytometry, and a monocyte adhesion assay was performed under flow conditions.

(A) Representative RT-qPCR experiment of MAN1C1 in HUVECS with the indicated irradiation dose and transfected with the indicated siRNA (4 days post-transfection, 2 days post-irradiation). Scatter with bar graphs show the fold change in gene expression, for which the expression in non-irradiated cells transfected with a non-targeted siRNA (siNT) was set to 1. Levels of gene expression inhibition by siMAN1C1 compared to siNT are 89% for non-irradiated samples and 91% for samples irradiated at 20 Gy. ACTB was used as the reference gene. Normalized expression data are represented as mean ± SEM derived from n = 3 technical replicates. One-way ANOVA test with Sidak correction. ns, not significant, $^{**}p \leq 0.01$, $^{***}p \leq 0.001$, $^{****}p \leq 0.0001$.

(B) Representative Western blot images performed with anti-MAN1C1 and anti-GAPDH antibodies on untreated samples, and samples treated with siNT or siMAN1C1 (15 µg per well). pTrip-LUC and p-Trip-MAN1C1 are control protein extracts from cells transduced with the corresponding lentiviral vectors (2 µg per well). IB, immunoblot.

(C) Quantification of FITC-Con A staining of non-irradiated and irradiated HUVECs after treatment with siNT or siMAN1C1. Fold change of FITC-Con A fluorescence intensity medians determined by flow cytometry. Data are represented as mean ± SEM of two independent experiments with n = 2-3 repeated measures within each replication. One-way ANOVA test with Sidak correction. $^{**}p \leq 0.01$, $^{***}p \leq 0.001$, $^{****}p \leq 0.0001$.

(D) Relative quantification and identification of endothelial N-glycans structure from endothelial proteins by HILIC-LC-MS/MS. Protein-linked N-glycans were extracted from unirradiated and 20 Gy-irradiated HUVECS treated with indicated siRNA before analysis. Percentages of the abundance of the 5 high-mannose N-glycan structures (upper panel) and the 4 complex N-glycan structures (lower panel) determined by HILIC-LC-MS. Quantified structures are shown on the left of the graphs. Data are represented as mean ± SEM of one experiment with n = 3 repeated measures. two-way ANOVA test with Tukey correction. $^{*}p \leq 0.05$, $^{****}p \leq 0.0001$.

(E) Interaction of THP-1 cells with a monolayer of HUVECs under flow conditions. Snapshots of representative film sequences used in the experiments illustrating the interactions between THP-1 and control (0 Gy) or 20 Gy-irradiated HUVECs treated with siNT or siMAN1C1 (2 days post-irradiation). After 5 min of a continuous flow of THP-1 cells fluorescently labeled with CellTracker Red CMPTX, a film of 10 images was recorded to determine the number of firmly adherent THP-1 cells (surrounded by white circles). The number of firmly adherent THP-1 cells is shown in yellow to illustrate this representative example. Scale bar, 100 µm.

(F) Quantification of firmly adherent THP-1 cells post-irradiation of HUVECs untreated and treated with siNT or siMAN1C1. Firmly adherent THP-1 cells were counted using the films recorded during the experiment. Data are represented as mean ± SEM of 3-5 independent experiments with at least n = 3 repeated measures from 15 different fields of observation within each lamella, for each sample. One-way ANOVA test with Sidak correction. $^{**}p \leq 0.01$, $^{***}p \leq 0.001$, $^{****}p \leq 0.0001$.

See also Figures S3, S4, and Video S1.

correlated with a statistically significant decrease in monocyte adhesion in irradiated HUVECs treated with siMAN1C1 compared to irradiated HUVECs treated with siNT (Figures 3C, 3D, and Video S2). A decrease in the number of arrested monocytes could also be observed in the non-irradiated condition between siNT- and siMAN1C1-treated cells (Figure 3D), but this difference is not statistically significant (adjusted p value = 0.0924).

To take this further, we wanted to know if MAN1C1 is involved in the transendothelial migration of monocytes. For this purpose, we used the same strategy of inhibition and overexpression of MAN1C1 in a model of transendothelial migration assessed using a real-time imaging system that we developed for this study.

Establishment of a model of transendothelial migration of monocytes assessed by real-time imaging

To this end, we analyzed the chemotactic transendothelial migration of THP-1 cells in real-time with the IncucyteS3 live cell analysis system. We first constructed, sorted, and cloned by flow cytometry a THP-1 line stably expressing the red fluorescent protein mKate2-N (Figure S5). With this cell line, the IncucyteS3 software reproducibly detects by segmentation the THP-1 cells that have migrated and adhere to the underside of the permeable membrane (Figure S5C). Using one of the selected THP-1 mKate2 clones, we developed the conditions for MCP1 chemotactic-induced migration through a monolayer of non-irradiated HUVECs. We show that hardly any migration occurs in the absence of MCP1 and is dependent on MCP1 concentration (Figure 4 and Video S3). We chose a concentration of 100 nM MCP1 to perform the following transendothelial migration assays. To investigate whether the assay efficiency could

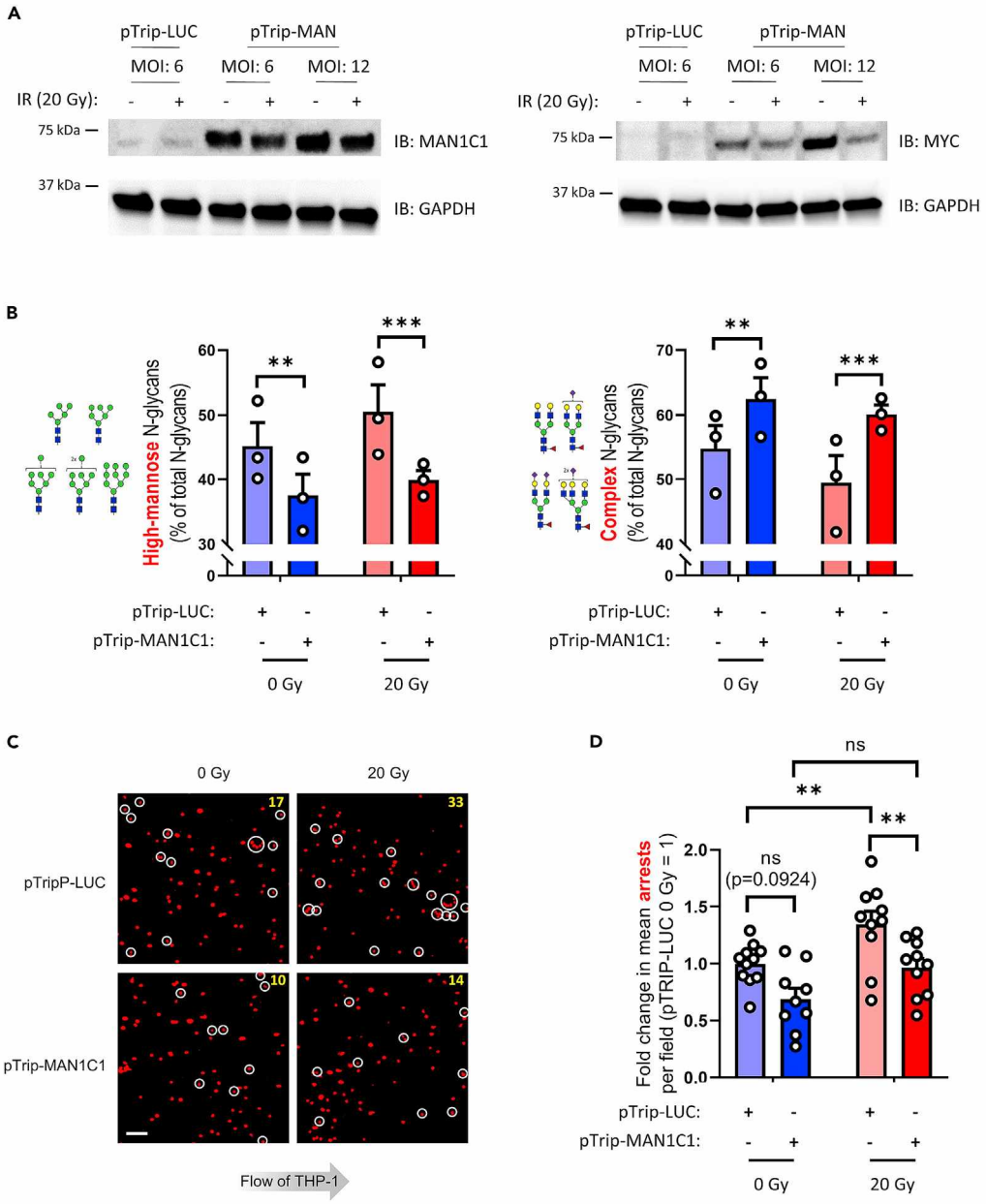

Figure 3. Decreased monocyte adhesion under flow conditions on a HUVEC monolayer overexpressing MAN1C1

HUVECs were transduced with pTrip-LUC or pTrip-MAN1C1. Four days post-transduction, cells were irradiated at 20 Gy, or not irradiated. Two days post-irradiation, proteins were collected for Western blot analysis, and a monocyte adhesion assay was performed under flow conditions.

(A) Representative Western blot images performed with anti-MAN1C1, anti-His Tag (MYC), and anti-GAPDH antibodies on samples treated with pTrip-LUC (at MOI 6) or pTrip-MAN1C1 (at MOI 6 and MOI 12) (2 µg of proteins per well). IB, immunoblot.

(B) Relative quantification and identification of endothelial N-glycans structure from endothelial proteins by HILIC-LC-MS/MS. Protein-linked N-glycans were extracted from unirradiated and 20 Gy-irradiated HUVECS treated with indicated lentiviral vector before analysis. Percentages of the abundance of the 5 high-mannose N-glycan structures (upper panel) and the 4 complex N-glycan structures (lower panel) determined by HILIC-LC-MS. Quantified structures are shown on the left of the graphs. Data are represented as mean ± SEM of one experiment with n = 3 repeated measures. two-way ANOVA test with Tukey correction. **p ≤ 0.01, ***p ≤ 0.001.

(C) Interaction of THP-1 cells with a monolayer of HUVECs under flow conditions. Snapshots of representative film sequences used in the experiments illustrating the interactions between THP-1 and control (0 Gy) or 20 Gy-irradiated

Figure 3. *Continued*

HUVECs transduced with pTrip-LUC or pTrip-MAN1C1 at Day 2 post-irradiation. After 5 min of a continuous flow of THP-1 cells fluorescently labeled with CellTracker Red CMPTX, a film of 10 images was recorded to determine the number of firmly adherent THP-1 cells (surrounded by white circles). The number of firmly adherent THP-1 cells is shown in yellow to illustrate this representative example. Scale bar, 100 μm.

(D) Quantification of firmly adherent THP-1 cells post-irradiation of HUVECs transduced with pTrip-LUC or pTrip-MAN1C1. Firmly adherent THP-1 cells were counted using the film sequences recorded in the experiment. Data are represented as mean ± SEM of two independent experiments with n = 4-6 repeated measures from 15 different fields of observation within each lamella, for each sample. One-way ANOVA test with Tukey correction. ns, not significant, $^{**}p \leq 0.01$.

See also Figures S3, S4, and Video S2.

be dependent on the THP-1 mKate2 clone, we tested three clones, obtained from three independent electroporations, for their ability to perform transendothelial migration. The results showed similar abilities between the three clones (Figure S6) and allowed us to choose the clone 5-H E5 to perform further experiments. We verified by flow cytometry that this clone exhibits the same characteristics as THP-1 in terms of the main surface markers expressed or not by classical monocytes (CD45, CD14, CD16, CX3CR1, CCR2). The results show that about 95% of THP-1 and THP-1 mKate2 clone 5-H E5 cells express CD45, CD14, and CCR2, but not CD16 and CX3CR1, as expected (Figure S7). Using the adhesion assay under flow conditions, we show that this clone retains the ability of THP-1 cells to adhere more to irradiated endothelial cells (Figure S7E).

Transendothelial migration of monocytes depends on HUVEC irradiation

We then investigated whether the transendothelial migration of monocytes is dependent on radiation exposure of HUVECs, a prerequisite for studying the players involved in radiation-induced immune cell recruitment. The results show a clear dose-dependent effect of radiation exposure on the passage rate of THP-1 through the layer of HUVECs (Figure 5 and Video S4). On the other hand, irradiation induces almost no passage of THP-1 in the absence of MCP1 (Figure 5B), suggesting that radiation-induced migration may be driven by an active process. We chose the 20 Gy dose for the rest of the transendothelial migration experiments, since it gives the greatest differential effect compared to the unirradiated conditions. We verified that irradiation at 20 Gy does not cause massive disruption of the endothelial barrier by a FITC-Dextran permeability assay performed using a chemotactic transendothelial migration plate (Figure S8). Although irradiation at 20 Gy increases the passage of Dextran by a factor of 4, it remains much lower than the passage of Dextran in the absence of an endothelial barrier which increases by a factor of 100 (Figure S8C). Finally, we checked that independent THP-1 mKate2 clones transmigrate similarly through the layer of HUVECs irradiated at 20 Gy, confirming that the 5-H E5 clone is suitable for the assay (Figure S6).

Transendothelial migration of monocytes is modified by the level of endothelial MAN1C1 expression

We used the same strategy as for the study of adhesion under flow to investigate the consequences of MAN1C1 inhibition/overexpression on monocyte transendothelial migration. First, treatment of HUVECs with siRNAs against MAN1C1 significantly decreases the rate of THP-1 passage in irradiated and non-irradiated conditions (Figure 6 and Video S5), despite incomplete inhibition of MAN1C1 expression with siRNA in lentiviral transduction experiments (by about 60% in this case) (Figure 6C). Next, we overexpressed MAN1C1 in HUVECs before performing a transendothelial migration assay. In contrast to the results obtained with MAN1C1 inhibition, the overexpression improves transendothelial migration, especially after irradiation (Figure 7 and Video S6). Because TNFα treatment had been shown to decrease MAN1C1 gene expression and increase expression of high-mannose N-glycans,[11] we wanted to test the consequences of this treatment on transendothelial migration. HUVECs treated with TNFα result in a significant decrease in THP-1 migration through the HUVEC layer (Figure S9), as observed upon silencing MAN1C1.

DISCUSSION

In a previous study, we showed that radiation exposure of endothelial cells downregulates MAN1C1 gene expression, increases the expression of high-mannose N-glycans trimmed by MAN1C1, and enhances monocyte adhesion under flow conditions, which is partly dependent on high-mannose N-glycans.[15] However, the role of MAN1C1 in monocyte adhesion to the vascular endothelium, especially after the irradiation of endothelial cells, remains elusive. In this study, we examined the consequences of modulating

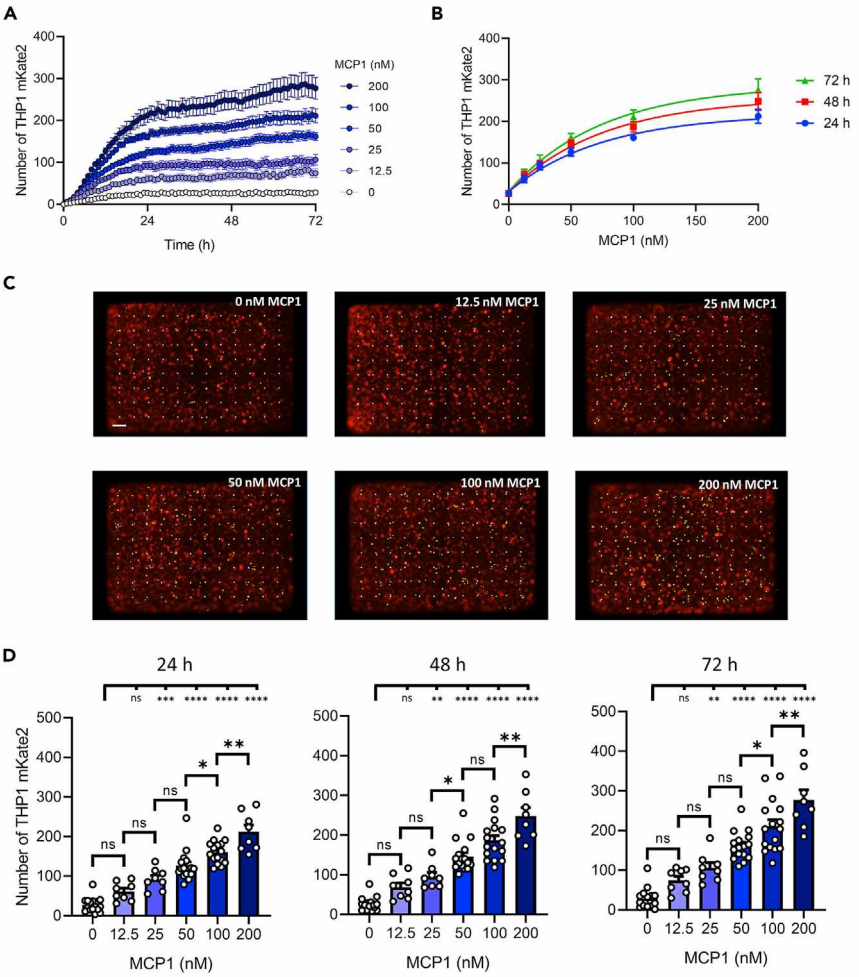

Figure 4. Transendothelial migration of THP-1 monocytes is dependent on the concentration of MCP1

HUVECs were seeded on wells of an Incucyte ClearView 96-Well Chemotaxis Cell Migration Plate. 72 h after seeding the HUVECs, THP-1 mKate2 clone 5-H E5 cells were added into the well, and culture medium containing 0, 12.5, 25, 50, 100, or 200 nM MCP1 was added to the wells of the plate reservoir. Plates were placed in the Incucyte S3 live cell analysis system in a cell culture incubator to monitor the transendothelial migration of monocytes every hour for 3 days

(A) Number of THP-1 mKate2 detected under the membrane by the Incucyte S3 module from 0 to 72 h after initiation of transendothelial migration and at different concentrations of MCP1 in the reservoir plate. Data are represented as mean ± SEM derived from n = 8-16 technical replicates.

(B) Number of THP-1 mKate2 detected under the membrane by the Incucyte S3 module as a function of MCP1 concentration at 24, 48, and 72 h after initiation of transendothelial migration. Curves were fitted by linear regression with exponential plateau and least squares fitting parameters. Data are represented as mean ± SEM derived from n = 8-16 technical replicates.

(C) Representative scans of the bottom of the permeable membrane of the chemotaxis cell migration plate 48 h after initiation of transendothelial migration illustrating MCP1-dependant passage of THP-1 mKate2 through a layer of HUVECs. Monocytes on top of the membrane, and therefore not having crossed the HUVECS layer, appear large and blurred, while monocytes that have crossed, adhering to the membrane, are well-focused and detected by the S3 Incucyte segmentation module (circled in yellow). Membrane pores are colored in white. Scale bar, 200 μm.

(D) Quantification of transendothelial migration of THP-1 mKate2 cells as a function of MCP1 concentration 24, 48, and 72 h after initiation of the transmigration. The experiment was repeated twice. Data are represented as mean ± SEM derived from n = 8-16 technical replicates. One-way ANOVA test with Tukey correction. ns, not significant, *$p \leq 0.05$, **$p \leq 0.01$, ***$p \leq 0.001$, ****$p \leq 0.0001$.

See also Figures S5, S6, S7, and Video S3.

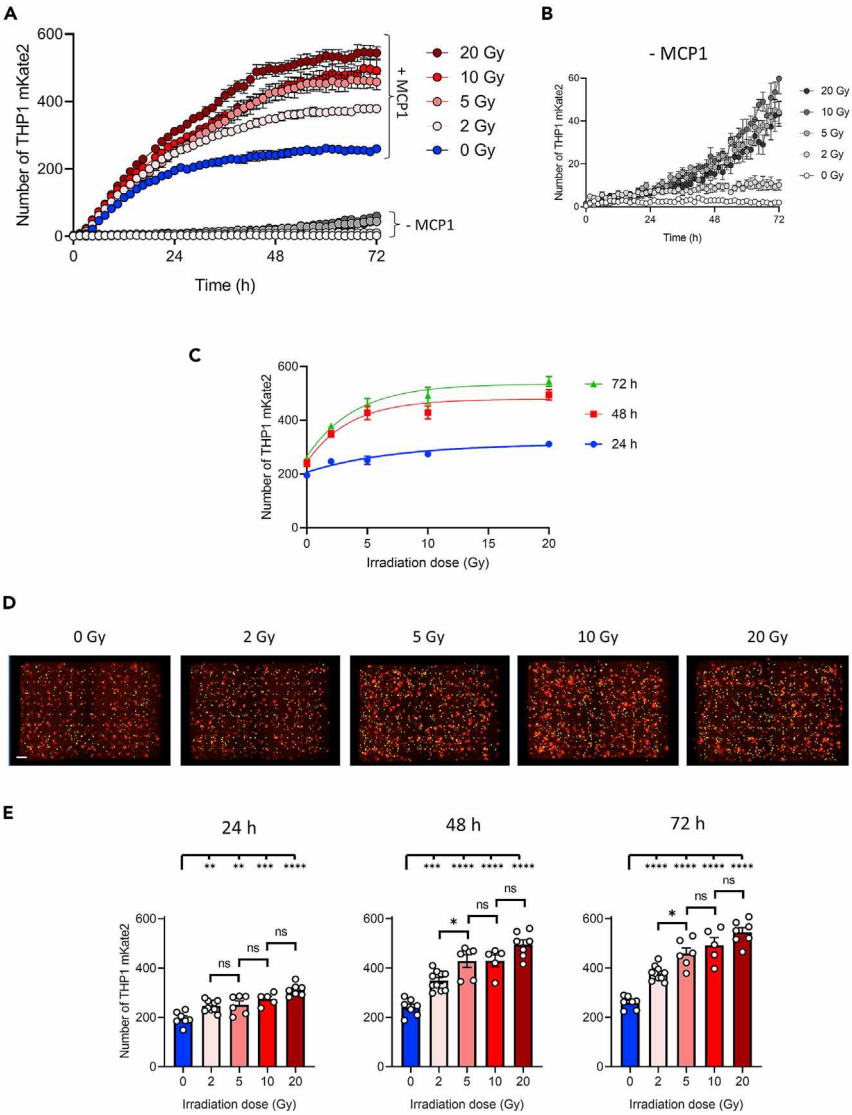

Figure 5. Transendothelial migration of THP-1 monocytes is dependent on the radiation dose

HUVECs were seeded on wells of an Incucyte ClearView 96-Well Chemotaxis Cell Migration Plate. 24 h after seeding HUVECs, the plates were irradiated at 0, 2, 5, 10, or 20 Gy. 48 h after irradiation, THP-1 mKate2 clone 5-H E5 cells were added to the wells, and culture medium containing 100 nM MCP1 was added to the wells of the plate reservoir. Plates were placed in the Incucyte S3 live cell analysis system in a cell culture incubator to monitor the transendothelial migration of monocytes every 1.5 h for 3 days

(A) Number of THP-1 mKate2 detected under the membrane by the Incucyte S3 module from 0 to 72 h after initiation of transendothelial migration and after irradiation of HUVECs at different doses, in the absence (-MCP1) or in the presence (+MCP1) of 100 nM MCP1 in the wells of the reservoir plates. Data are represented as mean ± SEM derived from n = 5-8 technical replicates.

(B) Number of THP-1 mKate2 detected under the membrane by the Incucyte S3 module from 0 to 72 h after initiation of transendothelial migration and after irradiation of HUVECs at different doses, in the absence of MCP1. Data are represented as mean ± SEM derived from n = 5-8 technical replicates.

(C) Number of THP-1 mKate2 detected under the membrane by the Incucyte S3 module as a function of radiation dose 24, 48, and 72 h after initiation of transendothelial migration in the presence of 100 nM MCP1 in the wells of the reservoir plates. Curves were fitted by linear regression with exponential plateau and least squares fitting parameters. Data are represented as mean ± SEM derived from n = 5-8 technical replicates.

(D) Representative scans of the bottom of the permeable membrane of the chemotaxis cell migration plate 48 h after initiation of transendothelial migration illustrating the radiation dependence of the passage of THP-1 mKate2 cells through a layer of HUVECs in the presence of 100 nM MCP1 in the wells of the reservoir plates. Monocytes on top of the

Figure 5. *Continued*

membrane, and therefore not having crossed the HUVECS layer, appear large and blurred, while monocytes that have crossed, adhering to the membrane, are well-focused and detected by the S3 Incucyte segmentation module (circled in yellow). Membrane pores are colored in white. Scale bar, 200 μm.

(E) Quantification of transendothelial migration of THP-1 mKate2 cells as a function of radiation dose 24, 48, and 72 h after initiation of the transmigration in the presence of 100 nM MCP1 in the wells of the reservoir plates. The experiment was repeated twice. Data are represented as mean ± SEM derived from n = 5-8 technical replicates. One-way ANOVA test with Tukey correction. ns, not significant, *p ≤ 0.05, **p ≤ 0.01, ***p ≤ 0.001, ****p ≤ 0.0001.

See also Figures S6, S8, and Video S4.

α-mannosidase MAN1C1 expression on the interactions between THP-1 monocytes and HUVECs under irradiation. To this end, we developed and used two real-time imaging *in vitro* models of (i) adhesion under flow conditions and (ii) transendothelial migration. The major finding of this study suggests that MAN1C1 regulates the interactions between THP-1 and HUVECs in the context of irradiation. Hence, we propose a role for endothelial MAN1C1 in the recruitment of monocytes, particularly in the step of adhesion to the endothelium.

We show that ionizing radiation downregulates the expression of MAN1C1 protein, reinforcing the hypothesis that this enzyme plays a role in high-mannose N-glycan-dependent radiation-induced monocyte adhesion. Using *in silico* pathway analysis, we identify that this regulation could take place through TNFα, IL1B and/or TGF-β signaling pathways which are induced by radiation exposure[16–22] and have been linked to negative regulation of MAN1C1.[11,20] It might be interesting to explore the involvement of the NF-κB pathway, which is, in particular, involved in radiation-induced inflammation in regulating cytokines,[23] to know if the expression of the MAN1C1 gene could be more precisely regulated by this pathway. On the other hand, radiation-induced ER stress, which has been documented in endothelial cells including HUVECs,[24,25] is a plausible hypothesis to explain the glycosylation changes we observed. To better understand the underlying mechanisms involved in monocyte adhesion by irradiated endothelial cells, it will be important to continue this work by studying the pathways responsible for the modification of MAN1C1 expression after irradiation.

These results support the theory that radiation-induced downregulation of MAN1C1 is involved in monocyte adhesion to irradiated endothelial cells. This could take place by increasing the abundance of endothelial high-mannose N-glycans, which have been shown to drive monocyte adhesion.[11,15] Our results show that MAN1C1 gene silencing increases the abundance of high-mannose N-glycans, improves the adhesion rate of monocytes on endothelial cells under flow conditions and decreases radiation-induced transendothelial migration of monocytes. Furthermore, overexpression of MAN1C1 produces exactly the opposite effect on high-mannose N-glycans, monocyte adhesion, and transmigration, supporting the results obtained with MAN1C1 silencing.

Given that, on the one hand, irradiation leads to a decrease in MAN1C1 expression and an increase in high mannose N-glycans expression, which we had previously shown to be at least partially responsible for the radiation-induced increase in monocyte adhesion under flow conditions,[15] and that, on the other hand, irradiation leads to increased transendothelial migration, we expected that siRNA treatment against MAN1C1 would lead to increased transendothelial migration. However, we observed the opposite effect. These results suggest that, under our experimental conditions, the inhibition of transendothelial migration by MAN1C1 silencing could be due to the increased abundance of high-mannose N-glycans, which we demonstrated by LC-MS/MS, which would retain monocytes on the surface of endothelial cells and prevent them from migrating through the layer of HUVECs. On the other hand, we show that the treatment of HUVECs with TNFα reduces transendothelial migration, in line with the results of MAN1C1 silencing. Previous studies had shown that the treatment of HUVECs with TNFα leads to an increase in high-mannose N-glycans and a decrease in MAN1C1 gene expression,[9,11,13] as does MAN1C1 inhibition in our experiments. Thus, our results showing the functional consequences of TNFα treatment on the transendothelial migration of THP-1 strengthens the hypothesis of a role for MAN1C1 in the regulation of monocyte-endothelial cell interactions. Regarding the effects of irradiation, this would be a mechanism involving several players in addition to the increase in high-mannose N-glycans, so that transendothelial migration would remain higher despite MAN1C1 silencing.

There are four class I α-mannosidases in humans: one ER α-mannosidase (MAN1B1) and three Golgi apparatus α-mannosidases (MAN1A1, MAN1A2, MAN1C1).[26] In this study, we focused on MAN1C1 because it

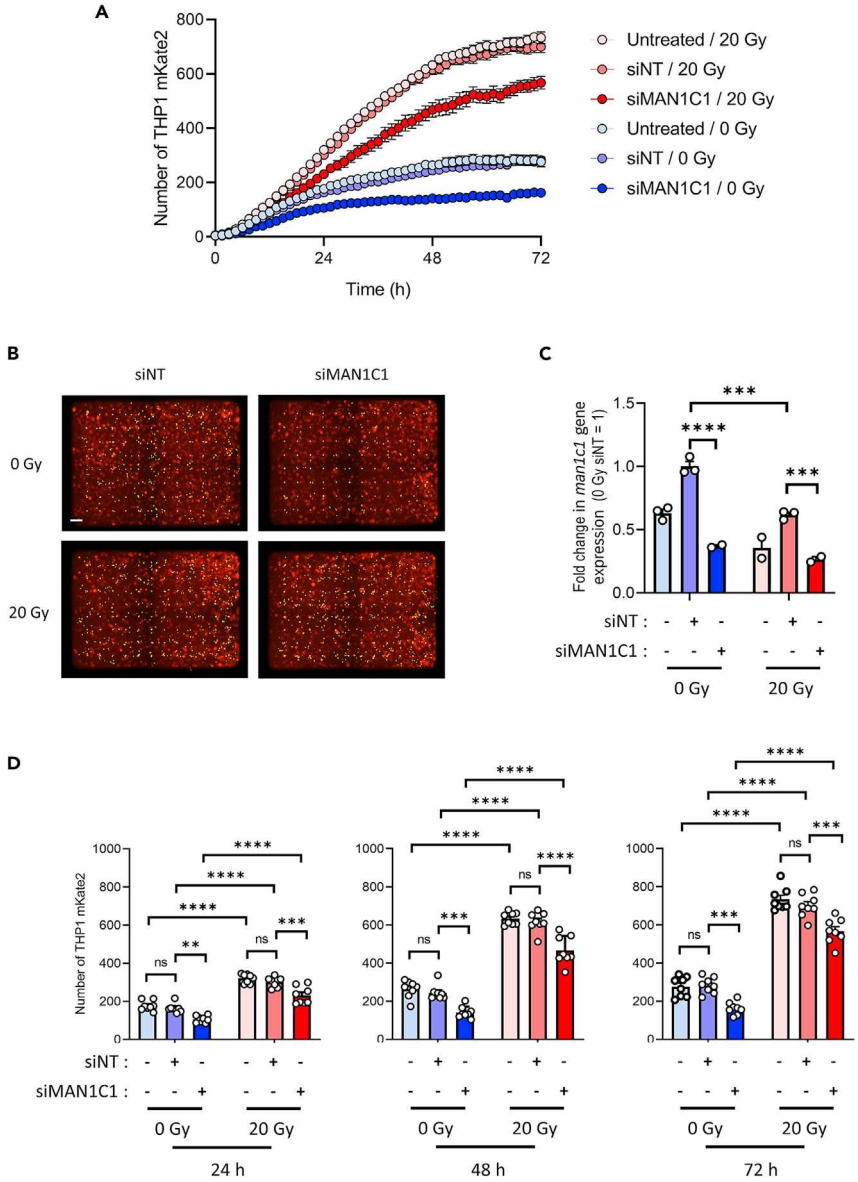

Figure 6. Decreased transendothelial migration of THP-1 monocytes on a HUVEC monolayer treated with siRNA against MAN1C1

HUVECs were untreated or transfected with siRNA against MAN1C1 (siMAN1C1) or with non-targeted siRNA (siNT) for 3 days. Cells were then seeded on 6-well plates for RT-qPCR analysis or wells of an Incucyte ClearView 96-Well Chemotaxis Cell Migration Plate for transendothelial migration assay. One day after seeding, the cells were irradiated at 20 Gy, or not irradiated. Two days post-irradiation, RNAs were collected for RT-qPCR analysis and a transendothelial migration assay was performed. 48 h after irradiation, THP-1 mKate2 clone 5-H E5 cells were added into the wells, and culture medium containing 100 nM MCP1 was added to the wells of the plate reservoir. Plates were placed in the Incucyte S3 live cell analysis system in a cell culture incubator to monitor the transendothelial migration of monocytes every 1.5 h for 3 days

(A) Number of THP-1 mKate2 detected under the membrane by the Incucyte S3 module from 0 to 72 h after initiation of transendothelial migration and after irradiation of untreated or transfected HUVECs with siRNA in the presence of 100 nM MCP1 in the wells of the reservoir plates. Data are represented as mean ± SEM derived from n = 8 technical replicates.

(B) Representative scans of the bottom of the permeable membrane of the chemotaxis cell migration plate 48 h after initiation of transendothelial migration in the presence of 100 nM MCP1 in the wells of the reservoir plates. Monocytes on top of the membrane, and therefore not having crossed the HUVECS layer, appear large and blurred, while monocytes that have crossed, adhering to the membrane, are well-focused and detected by the S3 Incucyte segmentation module (circled in yellow). Membrane pores are colored in white. Scale bar, 200 μm.

Figure 6. *Continued*

(C) A representative RT-qPCR experiment with the indicated irradiation dose and transfected with the indicated siRNA (4 days post-transfection, 2 days post-irradiation). Scatter with bar graphs show the fold change in gene expression, for which the expression in non-irradiated cells transfected with a non-targeted siRNA (siNT) was set to 1. Levels of gene expression inhibition by siMANC1 compared to siNT were around 60%. ACTB was used as the reference gene. Normalized expression data are represented as mean ± SEM derived from n = 2-3 technical replicates. One-way ANOVA test with Sidak correction. ***p ≤ 0.001, ****p ≤ 0.0001.

(D) Quantification of transendothelial migration of THP-1 mKate2 cells as a function of siRNA treatment and radiation dose 24, 48, and 72 h after initiation of the transmigration in the presence of 100 nM MCP1 in the wells of the reservoir plates. The experiment was repeated twice. Data are represented as mean ± SEM derived from n = 8 technical replicates. One-way ANOVA test with Sidak correction. ns, not significant, *p ≤ 0.05, **p ≤ 0.01, ***p ≤ 0.001, ****p ≤ 0.0001. See also Video S5.

was the only gene to be differentially expressed following irradiation in endothelial cells *in vitro*.[15] However, in this earlier work, it was shown that MAN1A1 and MAN1B1 genes are downregulated in the whole irradiated intestine, indicating that other class I α-mannosidases can be modulated by ionizing radiation. α-mannosidases are essential in the N-glycan biosynthetic chain. They work together to trim high-mannoses N-glycans and allow the maturation of N-glycans into hybrid and complex oligosaccharides.[10] Because these changes affect cell growth, cell-cell interactions, cell motility, and protein phosphorylation, the activity of these enzymes must be tightly regulated.[27] Abnormalities in the expression of these enzymes can lead to various diseases, including cancer. In particular, MAN1C1 potentially acts as a tumor suppressor as inhibition of its expression promotes the dissemination of cancer cells through increased cell-cell interactions.[28,29] Our results suggest that by decreasing MAN1C1 expression and increasing cell-cell interactions, irradiation may promote the establishment of a pro-tumoral environment.

Adhesion molecules play a key role in cell migration across the vascular endothelium. Ionizing radiation drives a persistent upregulation of ICAM-1 expression in endothelial cells *in vitro*[30] and increases adhesiveness of human aortic endothelial cells.[31] It was also shown that ICAM-1 deficient mice no longer showed inflammatory cell infiltration in the irradiated lung.[32] High-mannose N-glycans on ICAM-1 result in THP-1 monocyte adhesion independent of ICAM-1 and E-selectin expression,[11] as well as primary monocyte rolling and adhesion.[13,33] Previous studies have shown the functional consequences of increased high-mannose ICAM-1, which selectively recruits nonclassical/intermediate ($CD16^+$) over classical ($CD16^-$) monocytes in a Mac-1-dependent manner.[34] In our study, THP-1 cells exhibit cell surface markers of classical monocytes ($CCR2^+$, $CD14^+$, $CD16^-$), suggesting that it would be necessary to investigate the interaction of primary monocytes and subsets of monocytes using our *in vitro* models. Studies have shown that the high-mannose ICAM-1 glycoform is present in mouse and human atherosclerotic lesions[12,35] and positively correlates with macrophage content in these lesions. However, it is not known whether recruitment is exclusively dependent on ICAM-1. On the other hand, the surface proteins that exhibit high-mannose N-glycan contents are not known in the context of irradiation, much broader stress than TNFα treatment alone.

Overall, this research supports the theory that radiation-induced downregulation of, at least, MAN1C1 is involved in monocyte adhesion to irradiated endothelial cells through the increased expression of high-mannose N-glycans. Nevertheless, the role of MAN1C1 and high-mannose N-glycans in the recruitment of monocytes warrants further investigation *in vivo*. Future studies will investigate changes in endothelial cell glycosylation *in vivo* and determine whether irradiation does indeed down-regulate endothelial MAN1C1 and up-regulate high-mannose N-glycans. It will also be necessary to determine whether these glycosidic structures play a key role in monocyte recruitment, and, possibly, which monocyte subtypes are recruited in this way. Last, it will be interesting to determine whether this recruitment influences radiation-induced pathologies and tumor control in the context of radiation therapy. In this case, an interesting direction will be to interfere with this recruitment pathway by using available or under-development molecules that target high-mannose N-glycans.[9,36]

STAR★METHODS

Detailed methods are provided in the online version of this paper and include the following:

- KEY RESOURCES TABLE
- RESOURCE AVAILABILITY
  - Lead contact

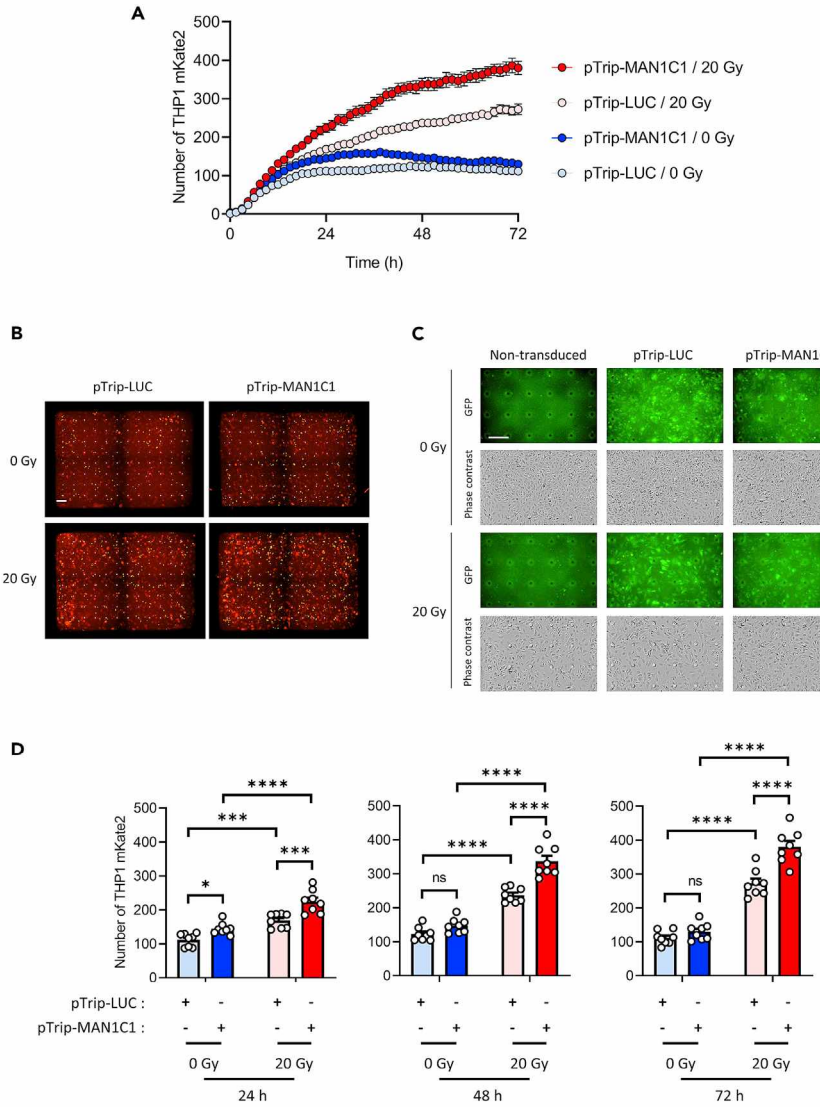

Figure 7. Increased transendothelial migration of THP-1 monocytes on a HUVEC monolayer overexpressing MAN1C1

HUVECs were incubated with pTrip-LUC or pTrip-MAN1C1 lentiviral particles for 2 days and amplified. Fourteen days post-transduction, cells were seeded on 6-well plates for Western blot analysis or wells of an Incucyte ClearView 96-Well Chemotaxis Cell Migration Plate for transendothelial migration assay. One day after seeding, the cells were irradiated at 20 Gy, or not irradiated. Two days post-irradiation, proteins were collected for Western blot analysis and a transendothelial migration assay was performed. 48 h after irradiation, THP-1 mKate2 clone 5-H E5 cells were added into the wells, and culture medium containing 100 nM MCP1 was added to the wells of the plate reservoir. Plates were placed in the Incucyte S3 live cell analysis system in a cell culture incubator to monitor the transendothelial migration of monocytes every 1.5 h for 3 days

(A) Number of THP-1 mKate2 detected under the membrane by the Incucyte S3 module from 0 to 72 h after initiation of transendothelial migration and after irradiation of transduced HUVECs with lentiviral vectors in the presence of 100 nM MCP1 in the wells of the reservoir plates. Data are represented as mean ± SEM derived from n = 8 technical replicates.

(B) Representative scans of the bottom of the permeable membrane of the chemotaxis cell migration plate 48 h after initiation of transendothelial migration in the presence of 100 nM MCP1 in the wells of the reservoir plates. Monocytes on top of the membrane, and therefore not having crossed the HUVECS layer, appear large and blurred, while monocytes that have crossed, adhering to the membrane, are well-focused and detected by the S3 Incucyte segmentation module (circled in yellow). Membrane pores are colored in white. Scale bar, 200 μm.

(C) Representative phase contrast and fluorescence (eGFP) images of non-transduced and transduced HUVECs with pTrip-LUC or pTrip-MAN1C1 at the time of initiation of transendothelial migration. Scale bar, 200 μm.

Figure 7. *Continued*
(D) Quantification of transendothelial migration of THP-1 mKate2 cells as a function of lentiviral vector treatment and radiation dose 24, 48, and 72 h after initiation of the transmigration in the presence of 100 nM MCP1 in the wells of the reservoir plates. The experiment was repeated twice. Data are represented as mean ± SEM derived from n = 8 technical replicates. One-way ANOVA test with Sidak correction. ns, not significant, *p ≤ 0.05, ***p ≤ 0.001, ****p ≤ 0.0001. See also Figure S9 and Video S6.

SUPPLEMENTAL INFORMATION

Supplemental information can be found online at https://doi.org/10.1016/j.isci.2022.105482.

ACKNOWLEDGMENTS

We are grateful to Dr. Philippe Peron (Sanofi-Aventis, Chilly-Mazarin, France) for his availability and his precious advice on the endothelial transmigration assay, and to Dr Françoise Pflumio (UMR Stabilité Génétique, Cellules Souches et Radiations, CEA, Fontenay-aux-Roses, France) for making the lentivirus cell culture laboratory at the IRCM (CEA, Fontenay-aux-Roses, France) available. We thank Dr. Jérome Lebeau (IRCM, CEA, Fontenay-aux-Roses, France) for his help in flow cytometry and Dr Jan Baijer (IRCM, CEA, Fontenay-aux-Roses, France) for making the IRCM cytometry platform available. We are also grateful to Plateforme PAGés (US 41 - UAR 2014 – PLBS) (université de Lille, France) for its valuable contribution. This work is supported by Electricité de France (Groupe Gestion Projet Radioprotection) and the Institut de Radioprotection et de Sûreté Nucléaire (ROSIRIS program). The funding agencies were not involved in any research plan relative to the study design, data collection and analysis, decision to publish, or drafting of the article.

AUTHOR CONTRIBUTIONS

S.L. and O.G. conceived and designed the experiments. D.B. supervised the lentiviral vector constructions. S.L., A.F.L, K.B., M.Q., E.B., G.P., J.D., N.D., N.Y., L.D., C.H., V.B., G.T., and O.G. performed experiments. S.L., D.B., G.P., N.Y., L.D., and O.G. wrote the original article. S.L., N.Y., L.D., F.A., V.P., A.F., F.M., and O.G. reviewed and edited the article. Funding acquisition was done by F.M. and O.G. O.G. supervised the project. All authors contributed to the article.

DECLARATION OF INTERESTS

The authors declare no competing interests.

Received: April 1, 2022
Revised: October 6, 2022
Accepted: October 28, 2022
Published: December 22, 2022

REFERENCES

1. François, A., Milliat, F., Guipaud, O., and Benderitter, M. (2013). Inflammation and immunity in radiation damage to the gut mucosa. Biomed Res. Int. *2013*, 123241.

2. Meziani, L., Deutsch, E., and Mondini, M. (2018). Macrophages in radiation injury: a new therapeutic target. Oncoimmunology *7*, e1494488.

3. Meziani, L., Mondini, M., Petit, B., Boissonnas, A., Thomas de Montpreville, V., Mercier, O., Vozenin, M.C., and Deutsch, E. (2018). CSF1R inhibition prevents radiation pulmonary fibrosis by depletion of interstitial macrophages. Eur. Respir. J. *51*, 1702120.

4. Mondini, M., Loyher, P.L., Hamon, P., Gerbé de Thoré, M., Laviron, M., Berthelot, K., Clémenson, C., Salomon, B.L., Combadière, C., Deutsch, E., and Boissonnas, A. (2019). CCR2-dependent recruitment of Tregs and monocytes following radiotherapy Is associated with TNFalpha-mediated resistance. Cancer Immunol. Res. *7*, 376–387.

5. Morrison, C. (2016). Immuno-oncologists eye up macrophage targets. Nat. Rev. Drug Discov. *15*, 373–374.

6. Guipaud, O., Jaillet, C., Clément-Colmou, K., François, A., Supiot, S., and Milliat, F. (2018). The importance of the vascular endothelial barrier in the immune-inflammatory response induced by radiotherapy. Br. J. Radiol. *91*, 20170762.

7. Wijerathne, H., Langston, J.C., Yang, Q., Sun, S., Miyamoto, C., Kilpatrick, L.E., and Kiani, M.F. (2021). Mechanisms of radiation-induced endothelium damage: emerging models and technologies. Radiother. Oncol. *158*, 21–32.

8. Schjoldager, K.T., Narimatsu, Y., Joshi, H.J., and Clausen, H. (2020). Global view of human protein glycosylation pathways and functions. Nat. Rev. Mol. Cell Biol. *21*, 729–749.

9. Regal-McDonald, K., and Patel, R.P. (2020). Selective recruitment of monocyte subsets by endothelial N-glycans. Am. J. Pathol. *190*, 947–957.

10. Stanley, P., Schachter, H., and Taniguchi, N. (2009). N-glycans. In Essentials of glycobiology, A. Varki, R.D. Cummings, J.D. Esko, H.H. Freeze, P. Stanley, C.R. Bertozzi, G.W. Hart, and M.E. Etzler, eds. (CSHL Press), pp. 101–114.

11. Chacko, B.K., Scott, D.W., Chandler, R.T., and Patel, R.P. (2011). Endothelial surface N-glycans mediate monocyte adhesion and are targets for anti-inflammatory effects of peroxisome proliferator-activated receptor gamma ligands. J. Biol. Chem. *286*, 38738–38747.

12. Scott, D.W., Chen, J., Chacko, B.K., Traylor, J.G., Jr., Orr, A.W., and Patel, R.P. (2012). Role of endothelial N-glycan mannose residues in monocyte recruitment during atherogenesis. Arterioscler. Thromb. Vasc. Biol. *32*, e51–e59.

13. Scott, D.W., Dunn, T.S., Ballestas, M.E., Litovsky, S.H., and Patel, R.P. (2013). Identification of a high-mannose ICAM-1 glycoform: effects of ICAM-1 hypoglycosylation on monocyte adhesion and outside in signaling. Am. J. Physiol. Cell Physiol. *305*, C228–C237.

14. McDonald, K.R., Hernandez-Nichols, A.L., Barnes, J.W., and Patel, R.P. (2020). Hydrogen peroxide regulates endothelial surface N-glycoforms to control inflammatory monocyte rolling and adhesion. Redox Biol. *34*, 101498.

15. Jaillet, C., Morelle, W., Slomianny, M.C., Paget, V., Tarlet, G., Buard, V., Selbonne, S., Caffin, F., Rannou, E., Martinez, P., et al. (2017). Radiation-induced changes in the glycome of endothelial cells with functional consequences. Sci. Rep. *7*, 5290.

16. Rubin, P., Johnston, C.J., Williams, J.P., McDonald, S., and Finkelstein, J.N. (1995). A perpetual cascade of cytokines postirradiation leads to pulmonary fibrosis. Int. J. Radiat. Oncol. Biol. Phys. *33*, 99–109.

17. Martin, M., Lefaix, J., and Delanian, S. (2000). TGF-beta1 and radiation fibrosis: a master switch and a specific therapeutic target? Int. J. Radiat. Oncol. Biol. Phys. *47*, 277–290.

18. Schaue, D., Kachikwu, E.L., and McBride, W.H. (2012). Cytokines in radiobiological responses: a review. Radiat. Res. *178*, 505–523.

19. Ishihara, H., Tsuneoka, K., Dimchev, A.B., and Shikita, M. (1993). Induction of the expression of the interleukin-1 beta gene in mouse spleen by ionizing radiation. Radiat. Res. *133*, 321–326.

20. Pabst, M., Wu, S.Q., Grass, J., Kolb, A., Chiari, C., Viernstein, H., Unger, F.M., Altmann, F., and Toegel, S. (2010). IL-1beta and TNF-alpha alter the glycophenotype of primary human chondrocytes *in vitro*. Carbohydr. Res. *345*, 1389–1393.

21. Hallahan, D.E., Virudachalam, S., Kuchibhotla, J., Kufe, D.W., and Weichselbaum, R.R. (1994). Membrane-derived second messenger regulates x-ray-mediated tumor necrosis factor alpha gene induction. Proc. Natl. Acad. Sci. USA *91*, 4897–4901.

22. Hallahan, D.E., Spriggs, D.R., Beckett, M.A., Kufe, D.W., and Weichselbaum, R.R. (1989). Increased tumor necrosis factor alpha mRNA after cellular exposure to ionizing radiation. Proc. Natl. Acad. Sci. USA *86*, 10104–10107.

23. Magné, N., Toillon, R.A., Bottero, V., Didelot, C., Houtte, P.V., Gérard, J.P., and Peyron, J.F. (2006). NF-kappaB modulation and ionizing radiation: mechanisms and future directions for cancer treatment. Cancer Lett. *231*, 158–168.

24. Kim, E.J., Lee, Y.J., Kang, S., and Lim, Y.B. (2014). Ionizing radiation activates PERK/eIF2alpha/ATF4 signaling via ER stress-independent pathway in human vascular endothelial cells. Int. J. Radiat. Biol. *90*, 306–312.

25. Panganiban, R.A.M., Mungunsukh, O., and Day, R.M. (2013). X-irradiation induces ER stress, apoptosis, and senescence in pulmonary artery endothelial cells. Int. J. Radiat. Biol. *89*, 656–667.

26. Herscovics, A. (2001). Structure and function of Class I alpha 1, 2-mannosidases involved in glycoprotein synthesis and endoplasmic reticulum quality control. Biochimie *83*, 757–762.

27. Molinari, M. (2007). N-glycan structure dictates extension of protein folding or onset of disposal. Nat. Chem. Biol. *3*, 313–320.

28. Li, H., Wang, G., Yu, Y., Jian, W., Zhang, D., Wang, Y., Wang, T., Meng, Y., Yuan, C., and Zhang, C. (2018). Alpha-1, 2-mannosidase MAN1C1 inhibits proliferation and invasion of clear cell renal cell carcinoma. J. Cancer *9*, 4618–4626.

29. Tu, H.C., Hsiao, Y.C., Yang, W.Y., Tsai, S.L., Lin, H.K., Liao, C.Y., Lu, J.W., Chou, Y.T., Wang, H.D., and Yuh, C.H. (2017). Up-regulation of golgi alpha-mannosidase IA and down-regulation of golgi alpha-mannosidase IC activates unfolded protein response during hepatocarcinogenesis. Hepatol. Commun. *1*, 230–247.

30. Gaugler, M.H., Squiban, C., van der Meeren, A., Bertho, J.M., Vandamme, M., and Mouthon, M.A. (1997). Late and persistent up-regulation of intercellular adhesion molecule-1 (ICAM-1) expression by ionizing radiation in human endothelial cells *in vitro*. Int. J. Radiat. Biol. *72*, 201–209.

31. Khaled, S., Gupta, K.B., and Kucik, D.F. (2012). Ionizing radiation increases adhesiveness of human aortic endothelial cells via a chemokine-dependent mechanism. Radiat. Res. *177*, 594–601.

32. Hallahan, D.E., and Virudachalam, S. (1997). Intercellular adhesion molecule 1 knockout abrogates radiation induced pulmonary

inflammation. Proc. Natl. Acad. Sci. USA *94*, 6432–6437.

33. Scott, D.W., Vallejo, M.O., and Patel, R.P. (2013). Heterogenic endothelial responses to inflammation: role for differential N-glycosylation and vascular bed of origin. J. Am. Heart Assoc. *2*, e000263.

34. Regal-McDonald, K., Xu, B., Barnes, J.W., and Patel, R.P. (2019). High-mannose intercellular adhesion molecule-1 enhances CD16(+) monocyte adhesion to the endothelium. Am. J. Physiol. Heart Circ. Physiol. *317*, H1028–H1038.

35. Regal-McDonald, K., Somarathna, M., Lee, T., Litovsky, S.H., Barnes, J., Peretik, J.M., Traylor, J.G., Jr., Orr, A.W., and Patel, R.P. (2020). Assessment of ICAM-1 N-glycoforms in mouse and human models of endothelial dysfunction. PLoS One *15*, e0230358.

36. Krautter, F., and Iqbal, A.J. (2021). Glycans and glycan-binding proteins as regulators and potential targets in leukocyte recruitment. Front. Cell Dev. Biol. *9*, 624082.

37. Nikitin, A., Egorov, S., Daraselia, N., and Mazo, I. (2003). Pathway studio–the analysis and navigation of molecular networks. Bioinformatics *19*, 2155–2157.

38. Shcherbo, D., Merzlyak, E.M., Chepurnykh, T.V., Fradkov, A.F., Ermakova, G.V., Solovieva, E.A., Lukyanov, K.A., Bogdanova, E.A., Zaraisky, A.G., Lukyanov, S., and Chudakov, D.M. (2007). Bright far-red fluorescent protein for whole-body imaging. Nat. Methods *4*, 741–746.

39. Li, M.Z., and Elledge, S.J. (2007). Harnessing homologous recombination *in vitro* to generate recombinant DNA via SLIC. Nat. Methods *4*, 251–256.

40. Sirven, A., Ravet, E., Charneau, P., Zennou, V., Coulombel, L., Guétard, D., Pflumio, F., and Dubart-Kupperschmitt, A. (2001). Enhanced transgene expression in cord blood CD34(+)-derived hematopoietic cells, including developing T cells and NOD/SCID mouse repopulating cells, following transduction with modified trip lentiviral vectors. Mol. Ther. *3*, 438–448.

41. Brunet de la Grange, P., Armstrong, F., Duval, V., Rouyez, M.C., Goardon, N., Romeo, P.H., and Pflumio, F. (2006). Low SCL/TAL1 expression reveals its major role in adult hematopoietic myeloid progenitors and stem cells. Blood *108*, 2998–3004.

42. Zufferey, R., Nagy, D., Mandel, R.J., Naldini, L., and Trono, D. (1997). Multiply attenuated lentiviral vector achieves efficient gene delivery *in vivo*. Nat. Biotechnol. *15*, 871–875.

STAR★METHODS

KEY RESOURCES TABLE

REAGENT or RESOURCE	SOURCE	IDENTIFIER
Chemicals, peptides, and recombinant proteins		
Dulbecco's Phosphate Buffered Saline	Thermo Fisher Scientific	Cat#: 14190-094
Dulbecco's Phosphate Buffered Saline, calcium, magnesium	Thermo Fisher Scientific	Cat#: 14040-117
EBM™-2, Endothelial Cell Growth Basal Medium-2	Lonza	Cat#: CC-3156
EGM™-2, MV Microvascular Endothelial Cell Growth Medium-2 SingleQuots™ Kit	Lonza	Cat#: CC-4147
RPMI 1640 Medium (ATCC Modification)	Thermo Fisher Scientific	Cat#: A10491-01
Gibco™ Fetal Bovine Serum, qualified, E.U.-approved, South America origin	Thermo Fisher Scientific	Cat#: 10270106
2-mercaptoethanol	Thermo Fisher Scientific	Cat#: 21985023
Trypsin-EDTA	Thermo Fisher Scientific	Cat#: 25300054
Trypan blue dye	Bio-Rad	Cat#: 145-0013
DMEM (high glucose, GlutaMAX™ Supplement, pyruvate)	Thermo Fisher Scientific	Cat#: 31966047
Penicillin-streptomycin	Thermo Fisher Scientific	Cat#: 15140122
Gibco™ Opti-MEM™ I Reduced Serum Medium	Thermo Fisher Scientific	Cat#: 31985-062
Nuclease-free water	Qiagen	Cat#: 129114
Ethanol absolute	VWR	Cat#: 20821.365
Dharmafect 1, Transfection Reagent	Thermo Fisher Scientific	Cat#: T-2001-02
mirVana™ miRNA Isolation kit	Thermo Fisher Scientific	Cat#: AM1560
High-Capacity cDNA Reverse Transcription Kit	Thermo Fisher Scientific	Cat#: 4368814
TaqMan™ Fast Universal PCR Master Mix (2X), no AmpErase™ UNG	Thermo Fisher Scientific	Cat#: 4366072
TaqMan™ Gene Expression Master Mix	Thermo Fisher Scientific	Cat#: 4370074
RIPA Lysis Buffer System	Santa Cruz Biotechnology	Cat#: sc-24948
cOmplete™, Mini, EDTA-free Protease Inhibitor Cocktail	Sigma-Aldrich	Cat#: 11836170001
PhosSTOP phosphatase inhibitor	Sigma-Aldrich	Cat#: 4906845001
Bicinchoninic Acid (BCA) Kit for Protein Determination	Sigma-Aldrich	Cat#: BCA1-1KT
4-15% Mini-PROTEAN TGX Precast Protein Gels	Bio-Rad	Cat#: 4561086
Nitrocellulose Membrane, Precut, 0.45 µm, 7 × 8.5 cm	Bio-Rad	Cat#: 1620145
EveryBlot Blocking Buffer	Bio-Rad	Cat#: 12010020
Multiple tags positive control (GST-DDDDDK-V5-HSV-HA-T7-Myc-S)	CliniSciences	Cat#: GTX130343-pro-25µg
SuperSIgnal West Pico PLUS Chemiluminescent Substrate	Thermo Fisher Scientific	Cat#: 34580
Rabbit Polyclonal MAN1C1 Antibody	Bio-Techne	Cat#: NBP2-14217

(*Continued on next page*)

Continued

REAGENT or RESOURCE	SOURCE	IDENTIFIER
Anti-Actin Antibody, clone C4	Merck Millipore	Cat#: MAB1501
His Tag Antibody	Bio-Techne	Cat#: MAB050-500
Goat Anti-Mouse IgG (H + L)-HRP Conjugate	Bio-Rad	Cat#: 1706516
Goat Anti-Rabbit IgG (H + L)-HRP Conjugate	Bio-Rad	Cat#: 1706515
MCP-1/MCAF human	Sigma-Aldrich	Cat#: SRP3109-20UG
Recombinant Human TNF-alpha	Bio-Techne	Cat#: 210-TA-100
Fibronectin bovine plasma	Sigma-Aldrich	Cat#: F1141-1MG
IncuCyte ClearView 96-well Chemotaxis Plate	Sartorius	Cat#: 4648
Cell Line NucleofectorTM Kit V	Lonza	Cat#: VCA-1003
Geneticin™ Selective Antibiotic (G418 Sulfate)	Thermo Fisher Scientific	Cat#: 10131035
Anti-CD45-PerCP antibody	BD Biosciences	Cat#: 345809
anti-CD16-PE antibody	BD Biosciences	Cat#: 560995
anti-CD14-FITC antibody	BD Biosciences	Cat#: 555397
anti-CX3CR1-BV605 antibody	BD Biosciences	Cat#: 744488
anti-CCR2-BV786 antibody	BD Biosciences	Cat#: 747855
Concavaline A - FITC	CliniSciences	Cat#: FL-1001
Fluorescein isothiocyanate–dextran	Sigma-Aldrich	Cat#: 46944-100MG-F
CellTracker™ Red CMTPX Dye	Thermo Fisher Scientific	Cat#: C34552
TO-PRO™-3 Iodide (642/661)	Thermo Fisher Scientific	Cat#: T3605
Hoechst 33258	Thermo Fisher Scientific	Cat#: H3569
pCMV6-HsMAN1C1-1-630-cMycFlag plasmid	Origene	Cat#: RC222009
pmKate2-N	Euromedex	Cat#: FP182
pCMV-VSV-G	Addgene	Cat#: 8454
Triton™ X-100	Sigma-Aldrich	Cat#: X100-100ML
Ammonium bicarbonate	Fluka analytical	Cat#: 40867-50G-F
Dithiothreitol	Sigma-Aldrich	Cat#: D9163-5G
Iodoacetamide bioultra	Sigma-Aldrich	Cat#: I1149-5G
Trichloroacetic acid	Sigma-Aldrich	Cat#: T9159-500G
PNGase F	New England Biolabs	Cat#: P0709S
Acetone	Carlo Erba	Cat#: 412501
Trypsin	Sigma-Aldrich	Cat#: T1005
Acetonitrile	Sigma-Aldrich	Cat#: 271004
Acetic acid	Carlo Erba	Cat#: 401422
Procainamide	Thermo Fisher Scientific	Cat#: 10733211
2-picoline borane	Santa Cruz Biotechnology	Cat#: sc-288295
DMSO	Sigma-Aldrich	Cat#: 276855-1L
Deposited data		
Plasmid pTRIP-MND-HsMAN1C1-1-630-cMycFlag-hPGK-EGFP	This paper	Addgene: 183505
Mammal (Anatomy; CellEffect™; DiseaseFx®; GeneticVariant; Viruses) version 12.4.0.5 (Updated Feb 27, 2022) database from Elsevier	Elsevier	www.elsevier.com/pathway-studio
Experimental models: Cell lines		
HUVEC – Human Umbilical Vein Endothelial Cells	Lonza	Cat#: C2519A
THP-1 cells	LGC Standards	Cat#: ATTC Number TIB-202

(*Continued on next page*)

Continued

REAGENT or RESOURCE	SOURCE	IDENTIFIER
293T cells	ATCC	Cat#: CRL-3216
Oligonucleotides		
Primers for TaqMan® Human gene expression assay: MAN1C1 - Assay ID: Hs01057229_m1	Thermo Fisher Scientific	Cat#: 4351372
Primers for TaqMan® Human gene expression assay: ACTB - Assay ID: Hs99999903_m1	Thermo Fisher Scientific	Cat#: 4331182
ON-TARGET plus Non-targeting Pool	Thermo Fisher Scientific	Cat#: D-001810-10-50
ON-TARGETplus Human MAN1C1 (557134) siRNA - Set of 4	Dharmacon	Cat#: LQ-020422-01-0005
*5′CTCACTCGGCGCGATCTGGATC*TG CCGCCGCGATCG-3′ (Forward)	Eurofins	Cat#: SP1333
5′CCCAACCCCGTGGGAATTCG TTAAACCTTATCGTCGTCATC CTTG-3′ (Reverse)	Eurofins	Cat#: SP1334
*5′CTCACTCGGCGCGATCTGG ATCC*GTCGCCACCATGGAA GACGCCAAAAAC-3′ (Forward)	Eurofins	Cat#: SP1311
*5′CCCAACCCCGTGGGAATTCG*TTA CACGGCGATCTTTCCGC-3′ (Reverse)	Eurofins	Cat#: SP1313
5′CACTCGGCGCGATCTGGATCCC GAATTCCCACGGGGTTG-3′ (Forward)	Eurofins	Cat#: SP1306
5′CACCATGGTGGCGACCGGTGG CTGGGGAGAGAGGTCGG-3′ (Reverse)	Eurofins	Cat#: SP1307
Software and algorithms		
GraphPad Prism version 8.1.1	GraphPad Software	www.graphpad.com
ImageJ version 1.52a software	National Institutes of Health	http://imagej.nih.gov/ij
Pathway Studio Web Mammal version 12.4.0.3	Nikitin et al., 2003	www.elsevier.com/pathway-studio
FlowJo v10.6.0	FlowJo LLC	https://www.flowjo.com
Compass DataAnalysis v4.4	Bruker	https://www.bruker.com/

RESOURCE AVAILABILITY

Lead contact

Further information and requests for resources and reagents should be directed to and will be fulfilled by the lead contact, Olivier Guipaud (olivier.guipaud@irsn.fr).

Materials availability

Plasmids generated in this study have been deposited with Addgene (Addgene: 183505).

Data and code availability

- All data reported in this paper will be shared by the lead contact upon request.
- This paper does not report original code.
- Any additional information required to reanalyze the data reported in this paper is available from the lead contact upon request.

EXPERIMENTAL MODEL AND SUBJECT DETAILS

Cells

Human umbilical vein endothelial cells (HUVECs, pooled donors, newborn, male/female mixed, product code C2519A, batch number 0000465419) from Lonza were grown at 37°C with 5% CO_2 in EBM™-2

Endothelial Cell Growth Basal Medium-2 (Lonza) containing 5% FBS, supplements and growth factors required for microvascular endothelial cells (EGM™-2 MV Microvascular Endothelial Cell Growth Medium-2 SingleQuots™ Kit, Lonza). THP-1 cells from ATCC (LGC Standards, ATTC Number TIB-202, batch number 63176297) were grown at 37°C with 5% CO2 in RPMI 1640 medium (ATCC modification), containing 10% heat inactivated FBS (Thermo Fisher Scientific), 1% penicillin-streptomycin (Thermo Fisher Scientific) and 50 mM 2-mercaptoethanol (Sigma-Aldrich). 293T cells from ATCC (ATTC Number CRL-3216) were cultured in DMEM (high glucose, GlutaMAX™ Supplement, pyruvate) (Thermo Fischer Scientific) containing 1% penicillin-streptomycin (Thermo Fischer Scientific) and 10% FBS (Thermo Fisher Scientific). Cells were authenticated by the suppliers and tested negative for mycoplasma, bacteria, yeast, and fungi, as guaranteed by the suppliers.

METHOD DETAILS

Irradiation procedure

Irradiation of HUVECs at doses of 2, 5, 10 or 20 Gy was performed using an Elekta Synergy® Platform delivering 4 MV X-rays at 2.5 Gy/min. Non-irradiated cells (0 Gy, control samples) were left for the same amount of time on a benchtop near the irradiation room. All irradiations were carried out at 90-100% cell confluence and the same number of population doublings (passage 3, corresponding to 9 to 12 population doublings) for experiments that did not use cells modified with siRNA or lentivirus. For experiments that required siRNA transfection or lentiviral transduction, cells were irradiated at passage 4 and up to passage 6, respectively. The cell culture media were replaced just before irradiation with fresh culture medium at 37°C. For long-term experiments (14- and 21-days post-irradiation), the culture medium was changed every week.

Estimation of cell number and viability

HUVECS were seeded on 6-wells plates. Five days after seeding, 90-100% confluence cells were not irradiated or irradiated at a single dose of 20 Gy. Two days later, cells were dissociated with trypsin-EDTA (Thermo Fisher Scientific) to estimate cell number and viability in the presence of Trypan blue dye (Bio-Rad) using the Bio-Rad TC20 automated cell counter.

Cell tracker labeling of THP-1 monocytes

For adhesion experiments under flow conditions, THP-1monocytes (10^6 cells/mL) were labeled with 1 μM CellTracker™ Red CMTPX (Thermo Fisher Scientific) in RPMI 1640 without FBS for 45 min at 37°C in the dark. After centrifugation (120 × g for 6 min), cells were resuspended in RPMI 1640 without FBS and incubated for 30 min at 37°C in the dark to remove unincorporated dye. Cells were centrifuged (120 × g for 6 min) and resuspended in EBM-2 MV medium without FBS at a concentration of 0.5 × 10^6 cells/mL and then used in an adhesion assay.

RNA isolation, reverse transcription and real-time quantitative PCR

Total RNAs were prepared using the mirVana miRNA isolation kit (Thermo Fisher Scientific). RNA concentrations were quantified on a NanoDrop ND-1000 apparatus (NanoDrop Technologies). Reverse transcription was performed with 1 μg RNA using the High-Capacity Reverse Transcription Kit (Thermo Fisher Scientific). Quantitative PCR was carried out on a 7900HT Fast-Real Time PCR system (Applied Biosystems) using pre-developed TaqMan Gene Expression Assays (Thermo Fisher Scientific). PCR fluorescent signals were normalized to a PCR fluorescent signal obtained from the housekeeping ACTB gene. Relative changes in gene expression were quantified using the ΔΔCT method.

Protein isolation and Western blot analysis

HUVECs were lysed at appropriate times using a RIPA Lysis Buffer System (Santa Cruz Biotechnology) containing cOmplete Mini EDTA-free Protease Inhibitor Cocktail (Sigma-Aldrich) and PhosSTOP phosphatase inhibitors (Sigma-Aldrich). Protein concentration was determined using a BCA Kit for protein determination (Sigma-Aldrich). Absorbance was measured in an Infinite M200 Pro (TECAN) microplate reader at 562 nm. Western blot was performed on 15 μg of total HUVEC proteins or 2 μg in case of lentiviral transduction. SDS-PAGE was carried out using MINI-PROTEAN TGX Precast gels 4-15% (Bio-Rad). Proteins were electro-transferred onto a nitrocellulose membrane (Bio-Rad) using a Trans-Blot® SD Semi-Dry Transfer Cell (Bio-Rad) at 0.8 mA/cm^2 during 1 h. After 10 min incubation in the EveryBlot Blocking Buffer (Bio-Rad), membranes were incubated with anti-MAN1C1 antibody (Biotechne) at a dilution of 1:500 for 12 h at 4°C, anti-ACTB antibody (Sigma-Aldrich) at a dilution of 1:10000, anti-GAPDH antibody at a dilution of

1:5000 (Sigma-Aldrich) or anti-His Tag antibody (Bio-Techne) for 1 h at room temperature (RT). Membranes were then incubated with Goat Anti-Rabbit IgG (H + L)-HRP Conjugate (Bio-Rad) or Goat Anti-Mouse IgG (H + L)-HRP Conjugate (Bio-Rad) at a dilution of 1:3000 for 1 h at RT. Finally, proteins were revealed using the SuperSignal West Pico PLUS Chemiluminescent Substrate (Thermo Fisher Scientific) using a ChemiDoc MP Imaging system (Bio-Rad). Quantification of band intensity was performed using ImageJ software.

Establishment of a regulation network of MAN1C1 by ionizing radiation

A network was built *in silico* using the Pathway Studio Web Mammal software, version 12.4, querying the Mammal (Anatomy; CellEffect™; DiseaseFx®; GeneticVariant; Viruses) version 12.4.0.5 (Updated Feb. 27, 2022) database from Elsevier (www.elsevier.com/pathway-studio)[37] Proteins mapped to the knowledge base were used to build protein networks. Interaction networks, established using the literature mining algorithm of Pathway Studio software, including selected neighbors, direct interactions, and shortest paths were added.

Creation of a THP-1 line expressing the mKate2-N red protein

Six independent electroporations (THP-1 mKate2-1 to -6) of 2×10^6 THP-1 cells were performed with 0.5 µg of pmKate2-N plasmid (Euromedex) using the Amaxa® Biosystems Nucleofector® II and an Amaxa® Cell line Nucleofector® Kit V (Lonza). The far-red fluorescent protein mKate2 expresses a super bright far-red fluorescence (excitation maximum, 588 nm; emission maximum, 633 nm).[38] THP-1 mKate2-N cells were grown in a classically used medium with the addition of selective geneticin antibiotic (Thermo Fisher Scientific) at 250 µg/mL. After amplification, cells were analyzed on a SORP LSR-II analyzer (BD Biosciences). Data were analyzed with FlowJo v10.6.0 (FlowJo LLC). For each sample, 90,000 to 100,000 cells were analyzed. For three independent electroporations (THP-1 mKate2 1, THP-1 mKate2 2 and THP-1 mKate2 5), 40,000 to 50,000 cells were sorted on a FACSAria II cell sorter (BD Biosciences) based on their level of fluorescence (medium or high) and single cells were seeded in 96-well culture plates. For each electroporation, two kinds of clone were sorted: THP-1 mKate2 X-M, for medium fluorescence, and THP-1 mKate2 X-H, for high fluorescence, where X is the electroporation number. The clones were then amplified and selected by fluorescence microscopy based on their fluorescence level by choosing the brightest red clones. Finally, three independent clones, named THP-1 mKate2 1-M C5 (1-M C5), THP-1 mKate2 2-H D11 (2-H D11) and THP-1 mKate2 5-H E5 (5-H E5), were selected and stored at −150°C.

Construction of lentiviral vectors

All enzymes are from New England Biolabs, antibiotics from Sigma-Aldrich and primers from Eurofins Genomics. The HsMAN1C1-1-630-cMyc-Flag encoding sequence was amplified by PCR from pCMV6-HsMAN1C1-1-630-cMycFlag plasmid (Origene). The forward (SP1333) and reverse (SP1334) primers harbor a 20-bp homology sequence with pTRIP-MND-hPGK-EGFP plasmid located apart from the *Bam*HI restriction site used for cloning. Upon amplification, resulting PCR product was subcloned by SLIC[39] in pTRIP-MND-hPGK-EGFP plasmid digested by *Bam*HI. The pTRIP-MND-hPGK-EGFP plasmid derived from pTRIP-DU3-EF1a plasmid[40] where the EF1a promoter was replaced by an MND promoter to drive gene expression[41] generating pTRIP-MND-EGFP. Then, to obtain an independent expression of EGFP, an hPGK promoter sequence was amplified with SP1306 and SP1307 from pVP81-eGFP plasmid (gift from F. Pflumio, UMR Stabilité Génétique, Cellules Souches et Radiations, CEA, Fontenay-aux-Roses, France) and cloned by SLIC in previously obtained plasmid digested by *Bam*HI. As a control, the luciferase encoding sequence was amplified with SP1311 and SP1313 from pTRIP-MND-Luciferase plasmid (gift from F. Pflumio, UMR Stabilité Génétique, Cellules Souches et Radiations, CEA, Fontenay-aux-Roses, France) and inserted by SLIC in pTRIP-MND-hPGK-EGFP plasmid digested by *Bam*HI. Positive clones were validated by DNA sequencing (Eurofins). The lentiviral vectors pTRIP-MND-HsMAN1C1-1-630-cMycFlag-hPGK-EGFP and pTRIP-MND-Luciferase-hPGK-EGFP were subsequently named pTrip-MAN1C1 and pTrip-LUC, respectively.

Production of lentiviral particles

293T cells were seeded in 175 cm^2 flasks with a density of 9,000 cells/cm^2 and cultured for 72 hours. Cells were co-transfected with 70 µg of pCMV-VSV-G (Addgene) and 100 µg of pCMVΔR8.91 (kindly provided by F. Pflumio, UMR Stabilité Génétique, Cellules Souches et Radiations, CEA, Fontenay-aux-Roses, France)[42] packaging plasmids, and 100 µg of the expression vector (pTrip-LUC or pTrip-MAN1C1) using the calcium phosphate method. The generated DNA precipitate was added to fresh medium and incubated with

previously plated cells. Upon 17 hours of incubation at 37°C with 5% CO_2, the medium was changed, and cells were cultured for additional 48 hours. Then, the culture medium containing viral particles was filtered on a 0.45 μm filter. The filtered suspension was centrifuged at 83,000 x g for 90 min at 4°C. Finally, the pellet was suspended in 200 μL PBS and stored at −80°C. Virus titration was performed by exposing 10^5 293T cells to viral particles in 24-well plates. Four serial 5-fold dilutions were tested for each lentivirus, starting with a volume of 0.25 μL of frozen initial suspension. After 72 hours of culture, cells were washed three times with PBS, harvested by flushing, and the percentage of fluorescent $eGFP^+$ cells was further determined by flow cytometry on a SORP LSR-II analyzer (BD Biosciences). The viral titer is based on the condition where less than 30% of cells are $eGFP^+$, according to the following formula: titer (particles per μL) = (number of plated cells x %age of $eGFP^+$ cells)/volume of virus in this condition.

Lentiviral transduction

HUVECs at 90-100% confluence were incubated for 2 days with lentivirus containing the pTRIP-MND-HsMAN1C1-1-630-cMycFlag-hPGK-EGFP or pTRIP-MND-Luciferase-hPGK-EGFP as the control condition using a multiplicity of infection (MOI) of 6 or 12 particles/cell. For monocyte adhesion under flow and transendothelial migration assays, HUVECs were dissociated with trypsin-EDTA (Thermo Fisher Scientific), washed with PBS and seeded at the appropriate density 2 days after transduction. Transduction efficiency was assessed by flow cytometry based on eGFP signal the day after functional tests.

siRNA transfection

HUVECs at 60-80% confluence were transfected with ON-TARGET plus human MAN1C1 siRNA (siMAN1C1) and ON-TARGET control pool siRNA NT (siNT) (GE Healthcare Dharmacon) as a control, using DharmaFECT (GE Healthcare Dharmacon) as the transfection reagent. Cells without any treatment were used for untreated conditions. To verify silencing by RT-qPCR, 6-well plates were seeded in parallel with similar culture and irradiation conditions.

Monocyte adhesion assay under flow conditions

Five days after seeding on a glass lamella, HUVECs at confluency were irradiated at 20 Gy. At different times post-irradiation, the lamella was placed in a flow chamber for videomicroscopy analysis.[15] THP-1 monocytes fluorescently labeled with CellTracker™ Red CMPTX were perfused through the flow chamber for a maximum time of 5 min at a constant wall shear rate of 75 s^{-1} and a constant flow rate of 150 μL/min using a syringe coupled to an electric pump (Harvard Apparatus). The entire experiment was visualized in real time at x20 magnification using a Rolera EM-C^2 camera (QImaging). Monocyte movements were recorded using MetaVue software (Molecular Devices). The full time-lapse video recorded the movement of monocytes using a frame rate of 30 frames per second with an exposure of 5 ms per frame. After 5 min of perfusion, 10-image time-lapse videos were recorded to determine the number of firmly adherent monocytes at 15 different locations along the glass lamella in the center of the flow. The time-lapse videos were subsequently analyzed by manual counting to determine the number of firmly adherent monocytes.

Transendothelial migration assay

Transendothelial migration assays were performed using the Incucyte™ ClearView™ 96-Well Chemotaxis Cell Migration Plate (Essen BioScience). 6,000 HUVECs per well were seeded in the top compartment on the permeable membrane previously coated with a 5 μg/mL fibronectin solution (Sigma Aldrich). The reservoir plate was filled with warm PBS. Cells were cultured for 24 h in standard culture conditions and then irradiated at the appropriate dose. Two days after irradiation, 5,000 THP-1 mKate2 cells in EGM™-2 medium were added to each well on the HUVECs layer. Just before starting the experiment, the bottom compartment was replaced with EGM2 medium containing or not containing MCP1 (Sigma Aldrich). Irradiated and non-irradiated chemotaxis plates were placed in the Incucyte S3 live cell analysis system (Essen BioScience) placed in a cell culture incubator to monitor the transmigration of monocytes. Each well of the plate was scanned using the chemotaxis module available on the Incucyte S3. Scans of the top and the bottom side of the permeable membrane were recorded in transmitted light and red fluorescence (800 ms exposure) using a x10 objective lens. Scans were scheduled every 30 min, 1 h or 1.5 h for a total time of 3 days. Analysis of the scans was performed using Incucyte software (Chemotaxis Migration Top/Bot analysis type) with the following analysis definition: for the phase, seed threshold of 50, grow threshold of 100, no clean-up, no area and eccentricity filters; for the red fluorescence, segmentation with a seed threshold (RCU) of 10^{-5}, a grow threshold of 50, an edge sensitivity of 0, no clean-up filter, area filter of minimum

20 μm^2 and maximum 600 μm^2, eccentricity filter of maximum 0.78, mean intensity filter of 0.1, no integrated intensity filter.

Flow cytometry analysis

FITC-Con A labeling

After dissociation with trypsin-EDTA (Thermo Fisher Scientific), cells were resuspended in 1 mL of PBS with Ca^{2+} and Mg^{2+} containing 5% FBS and stained with To-Pro-3 iodide (Thermo Fisher Scientific) and 10 μg/mL FITC-Con A lectin (CliniSciences) for 15 min on ice in the dark. Multiparametric analyses were performed on BD FACSCantoTM II (BD Biosciences) for data recording and data were analyzed using FlowJo 10.6.0 software (FlowJo LLC). To-Pro-3 fluorescence was collected on the APC channel to record living cell events. For these gated events, gating was done on size (FSC, forward scatter) and granulometry (SSC, side scatter) parameters. Last, the FITC-Con A signal was collected on the FITC channel. Results are presented as average median values of FITC-Con A fluorescence with at least 50,000 gated events per replica. All acquisitions and analyses were performed without compensation as FITC and To-Pro-3 signals do not overlap.

THP-1 and THP-1 mKATE2 surface staining

Cells were analyzed using the Aurora spectral flow cytometer (Cytek). To-Pro-3 was used to assess cell viability. Gating was done on size (FSC, forward scatter) and granulometry (SSC, side scatter) parameters and living cells (To-Pro-3 negative cells). Positive and negative populations for other markers were defined using fluorescence minus one (FMO) controls. Anti-CD45-PerCP, anti-CD16-PE, anti-CD14-FITC, anti-CX3CR1-BV605 and anti-CCR2-BV786 antibodies were purchased from BD Biosciences. Data analyses were performed on FlowJo 10.6.0 (FlowJo LLC).

Liquid chromatography–tandem mass spectrometry analysis of N-glycans

N-glycans release and labeling

After dissociation with trypsin-EDTA (Thermo Fisher Scientific), 3 to 5 million cells per sample were washed 3 times with 10 mL of PBS and stored at −80°C. The cells were suspended in 0.5 mL of 1% Triton X-100 (Sigma Aldrich) in 50 mM ammonium bicarbonate (AMBIC) (Sigma Aldrich) buffer, sonicated in an ice bath, and incubated at 37°C for 3 days. Proteins were reduced with 10 mM dithiothreitol (Sigma Aldrich) in 50 mM AMBIC buffer, followed by alkylation with 50 mM iodoacetamide (Sigma Aldrich), and incubated at 37°C for 1 hour. A solution of trichloroacetic acid (TCA) (Sigma Aldrich) wad added for the precipitation of proteins to a final concentration of 10% (w/v) and left at −20°C for 30 min. The protein pellet collected by centrifugation at 13,000 rpm for 10 min at 4°C was washed with 100% cold acetone (Carlo Erba) three times and dried under a stream of nitrogen. The pellet was resuspended in 200 μL of 50 mM AMBIC, and digested by adding two time 30 μL of 5 mg/mL trypsin (Sigma-Aldrich) at 37°C for 2 days. After trypsin inactivation at 100°C for 5 min, 62.5 U of Peptide:N-glycosidase F (PNGase F) (New England Biolabs) was added two time and incubated at 37°C for 24 h. The released N-glycans were separated from peptides on a C18 SPE cartridge (Interchim) activated with acetonitrile (Sigma-Aldrich) and equilibrated in 5% acetic acid (Carlo Erba). Samples were loaded and washed in the same solvent. N-glycans were recovered in the flow-through fraction and wash fraction, and dried. N-glycans were re-dissolved in the minimum amount of water. Labeling procainamide reagent (19.15 mg procainamide (Thermo Fisher Scientific), 22.4 mg 2-picoline borane (Santa Cruz Biotechnology), 0.5 mL DMSO (Sigma-Aldrich)/acetic acid(Carlo Erba) (7/3, v/v)) was added and incubated at 65°C for 2 hours. Then, 1 mL of acetonitrile 95% (v/v) was added. The labeled N-glycans was cleaned up by using Supelco HILIC cartridge (55465-U) (Sigma Aldrich). The cartridges were activated and equilibrated with 1 mL of water and 1 mL of acetonitrile 99%, successively. Samples were loaded and washed with 0.5 mL of acetonitrile 99%. The cartridges were washed 4 times with 1 mL of acetonitrile 99%. Finally, labeled N-glycans were eluted in a new tube with 100 μL of acetonitrile 5% (v/v) 4 times, then dried.

UHPLC-MS analysis

The dried procainamide labeled samples were dissolved in 50 μL of 78% acetonitrile (v/v) and analyzed by HILIC-LC-ESI-MS using Ultimate 3000 RSLC-nano system (Dionex/Thermo Fischer Scientific) coupled to an amaZon speed ETD ion trap (Bruker Daltonics). Ten microliters of sample were injected and separated on a AdvanceBio Glycan Mapping (300 Å, HILIC, 2.1 × 100 mm, 1.8 μm, Agilent) with 100 mM ammonium formate, pH 4.5, as solvent A and acetonitrile 100% as solvent B. Gradient conditions were: 0 min,

B 78%; 0 to 56.62 min, B 65.9%; 56.62 to 58.09 min, B 20%; 58.09 to 65.44 min, B 20%; 65.44 to 70.50 min, B 78%; 70.50 to 75.53 min, B 78% at a flow rate of 0.3 mL/min. Precursor ions were acquired in Xtreme Scan mode using a combination of auto-MS and Single Ion Monitoring scan modes in positive ion mode with a mass range of 100 to 3,000 m/z, capillary voltage 4.5 kV, desolvation temperature 200°C, desolvation gas flow 8 L/min. All fragmentations were performed by data-dependent auto-MS/MS in the positive mode. The obtained data were processed with Bruker Compass DataAnalysis v4.4.

TNFα stimulation

HUVECs were cultured for 24 h with a cell culture medium containing 10 μg/mL of recombinant human TNFα (Bio-Techne).

FITC-dextran permeability assay

A permeability assay was performed by using the fluorescein isothiocyanate-dextran (FITC-Dextran, Sigma-Aldrich) in EGM™-2 medium. FITC-Dextran at a concentration of 1 mg/mL was added to the top compartment of the Incucyte™ ClearView™ 96-Well Cell Migration Plate previously seeded with HUVECs and the reservoir plate was filled with PBS. Plates were incubated at 37°C in the dark for 3 hours. Fluorescence was measured at 535 nm in the PBS solution of the reservoir plate using the Infinite M200 Pro plate reader (TECAN).

QUANTIFICATION AND STATISTICAL ANALYSIS

Results are expressed as mean ± SEM. When the data meet the normality assumption (Shapiro-Wilk), we performed one-way ANOVA followed by multiple comparison tests (Tukey or Sidak). All p-values were corrected for multiple comparison tests (Tukey or Sidak). The type of test used is indicated in the figure legend for each data set. A p-value of <0.05 was considered statistically significant. *, $p \leq 0.05$; **, $p \leq 0.01$; ***, $p \leq 0.001$; ****, $p \leq 0.0001$ for the comparisons indicated, error bars represent standard error of means. The tests were performed using GraphPad Prism (GraphPad Software, Inc.) version 8.1.1 for Windows, which was also used to build the graphs.